What sets the heat content of Southern Ocean mode water formation regions?

Emma J. D. Boland[1], Daniel C. Jones[1], Andrew J. S. Meijers[1], and Simon A. Josey[2].

[1]British Antarctic Survey, High Cross, Madingley Road, Cambridge, United Kingdom
[2]National Oceanography Centre, European Way, Southampton, United Kingdom

Key Points:

- The heat content of SO MWFRs is most sensitive to local, recent heat flux changes and nonlocal wind stress changes on multi-year timescales.
- High sensitivity regions reveal source waters for the MWFRs and other sensitivities reveal dynamic links with boundary currents and the ACC.
- Perturbation experiments confirm an adjoint can predict the behavior of these regions as linear behaviour dominates on seasonal timescales.

Corresponding author: Emma J. D. Boland, `emmomp@bas.ac.uk`

Abstract

The Southern Ocean (SO) is a crucial region for the global ocean uptake of heat and carbon. There are large uncertainties in the observations of fluxes of heat and carbon between the atmosphere and the ocean mixed layer, which leads to large uncertainties in the amount entering into the global overturning circulation. In order to better understand where and when fluxes of heat and momentum have the largest impact on near-surface heat content, we use an adjoint model to calculate the linear sensitivities of heat content in SO mode water formation regions to surface fluxes. We find that the heat content of these regions is most sensitive to recent, local heat fluxes, and to non-local wind stress fluxes on the order of one to eight years previously. This is supported by the calculation of sensitivities to kinematic potential temperature changes, which reveal the sources of the mode water formation regions, and by sensitivities to dynamic potential temperature changes, which reveal dynamic links with boundary currents, the ACC, Kelvin and Rossby waves. A series of forward perturbation experiments in the fully non-linear model confirm that the adjoint model can accurately predict linear changes in heat content of fixed volume mode water formation regions. These experiments also highlight that non-linear effects can also be of importance, depending on the time and region investigated, and that the contribution of volume changes to heat content changes can be as large or larger than temperature changes.

The Southern Ocean is of crucial importance to the global ocean's uptake of carbon and heat. However, due to difficulties in making observations in such a remote and hostile environment, we currently don't know accurately how much heat and carbon enters the Southern Ocean from the atmosphere. Heat from the Southern Ocean gets locked away for hundreds to thousands of years in the globe's deep oceans, entering through a few key regions. We use a computer model to assess how the heat, fresh water, and wind energy entering through the surface of the Southern Ocean affects the heat of these key regions. We find that these regions are very sensitive to heat coming in through the surface directly over them, and that winds across a wider area of the Southern Ocean can affect the heat in them for several years. If we want to estimate the heat in these regions accurately, this information can be used to help us decide where and when it is important to measure heat and winds better.

1 Background

The Southern Ocean (SO) is home to the world's longest and strongest ocean current, the Antarctic Circumpolar Current (ACC), which encircles the globe free of continental barriers. Driven by strong wind and buoyancy forcing, the ACC transports climatically important tracers such as heat, salt, and CO_2 between the three major ocean basins. These forcings also create sloping density surfaces (isopycnals) which tilt upwards from north to south, bringing deep waters from around the globe to the surface. At the surface, air-sea interactions modify the properties of water masses. These modified waters then return to depth and into the other ocean basins as very dense bottom waters near the Antarctic continental shelf, or as lighter mode and intermediate waters north of the ACC (Lumpkin & Speer, 2007). This process of deep waters surfacing, being modified, and returning to depth is known as overturning (Marshall & Speer, 2012).

The Southern Ocean is of critical importance to the global oceanic uptake of heat and carbon, due in part to its powerful overturning circulation. Disproportionate to its relative size, it is responsible for more than 75% of the global ocean heat uptake and approximately 50% of the carbon uptake (Frölicher et al., 2015; Mikaloff Fletcher et al., 2006). Understanding these processes is crucial for increasing our understanding of the climate system as a whole – since the industrial revolution, global warming has been increasing the amount of heat and carbon in the Earth System, with roughly 30% of anthropogenic CO_2 emissions ending up in the ocean (Khatiwala et al., 2013), and over 93% of this excess heat being stored in the ocean (Levitus et al., 2012), with the SO dominating observations of global ocean warming (Roemmich et al., 2015).

Understanding what determines the time scales of Southern Ocean overturning and the properties of the waters transported is of crucial importance to future climate predictions, including the continued efficiency of the carbon sink (Landschützer et al., 2015; Le Quéré et al., 2018). The properties of the overturning circulation are affected by a range of processes, including variations in surface forcings, variations in the interactions of these forcings with ocean mixed layer properties, and variations in the draw-down of mixed layer properties into the ocean interior as mode, intermediate, and deep waters. Quantifying variations in surface forcings requires accurate measurements of these forcings. Unfortunately, such observations are scarce in the Southern Ocean, especially in the winter when sea ice hinders access to the region (Newman et al., 2015). This leads to poorly constrained reanalysis products and models, and thus a poor overall understanding of the overturning process. This work focuses on understanding how variations in surface forcings impacts on mode water formation regions within the mixed layer. This will provide insights into the influence of uncertainties in observations of surface forcings on estimates of mode water properties, as well as for estimating the impact of future changes in these forcings.

For this study, we use an adjoint model to try to understand the impact of surface forcings on the heat content of mode water formation regions (MWFRs). Adjoint models calculate linear sensitivities to quantities of interest known as ‘objective functions’, see section 2 for further details. Using the adjoint approach, one does not have to theorize what variable, when, or where, is the most relevant for setting your quantity of interest, as the sensitivities are calculated at all points in the model domain at multiple time lags. However, because the adjoint model is linear, it does not replace the need for full, non-linear simulations, as there are important processes that will not be captured in adjoint sensitivity fields. Adjoint models are thus best suited to looking at quantities one can expect to be largely controlled by linear effects, i.e. relatively large volumes and time periods. In this context, a linear effect might be the simple advection of a quantity such as heat, and a non-linear effect might be diffusion or parametrised mixing. For a more thorough discussion of adjoint models, including the setup used in this study, refer to section 2 in Jones et al. (2018) and references therein.

2 Experiment Design

For this study we use the ECCOv4 (release 2) ocean state estimate framework (Forget et al., 2015). This is a global $\sim 1^\circ$ ocean and sea ice setup of the MITgcm model (Adcroft, Campin, Hill, & Marshall, 2004) that spans 20 years from 1992 to 2011, with surface forcings and initial conditions that have been optimized to reduce misfits to observations. Details of the 4D-Var optimization process and the residual model-data misfit can be found in Forget et al. (2015). We choose to use this set-up as it not only provides a recent, well-constrained estimate of the Southern Ocean, but also because it can be easily modified to carry out adjoint sensitivity experiments, in which we examine the linear sensitivity of a quantity of interest to a set of model state variables and surface forcings.

An adjoint model, in this context, is one that starts from a quantity of interest (henceforth referred to as an ‘objective function’), such as the integrated temperature or salinity over a certain region, and linearly interpolates backwards in time between saved checkpoints of the forward non-linear model. This is in order to determine the linear sensitivity of the objective function to a range of specified model variables, such as surface fluxes or interior properties (e.g. potential temperature, mixing parameters). The objective function is normally the quantity of interest in a defined volume integrated over

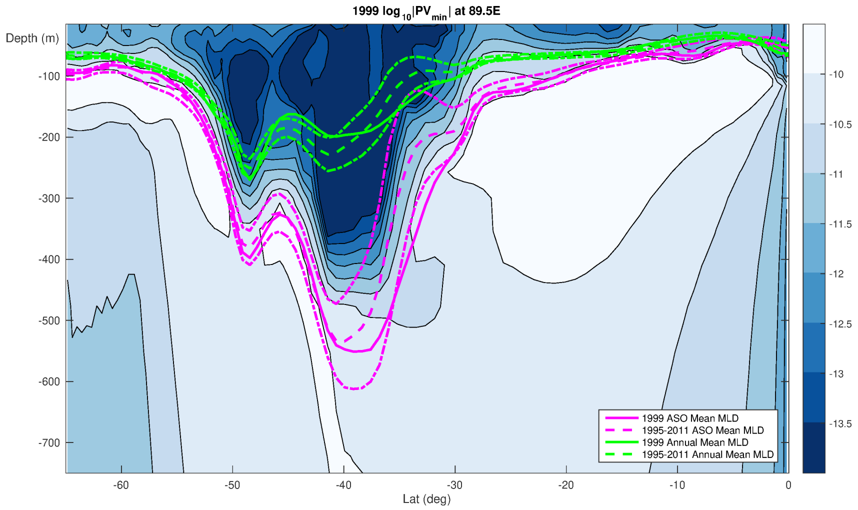

Figure 1. An example mode water formation region, characterized by low PV values, contained within the winter mixed layer: Latitude-depth plot of the absolute value of the 1999 minimum PV along 90°E in ECCOv4 r2, on a log scale (color). Also shown are the August-October (ASO) mean mixed-layer depth for 1999 (pink line) and 1995-2011 mean and standard deviations (pink dashed and dash-dotted lines) and the annual mean MLD for 1999 (green line) and 1995-2011 mean and standard deviations (green dashed and dash-dotted lines).

a specific time period in the full non-linear model. In a more traditional model study, one might start by choosing a model variable or variables theorized to impact one's quantity of interest, and then carry out a suite of perturbation experiments changing these variables by a range of magnitudes, locations, and/or times. By comparison with a control run, one then infers the sensitivity of the quantity of interest to the perturbation points in the model, simulation by simulation. In contrast, an adjoint model can produce in one single model run the linear sensitivity of one's quantity of interest to a range of model variables, at all points in the model domain, at multiple time lags.

For this study, our quantity of interest is the heat content of SO mode water formation regions. By definition, such water is characterized by low stratification (i.e. low PV values) (see e.g. Hanawa & Talley, 2001). Figure 1 shows a latitude-depth plot along 90°E (in the Indian sector of the Southern Ocean) of the minimum PV values for a representative year (1999) from the ECCOv4 r2 state estimate (notice the logarithmic color scale). There is a sharp lateral gradient in the minimum PV values just inside the winter mixed layer extent, and as such that the winter mixed layer extent captures the mode water formation pools we are interested in.

Three distinct mode water formation pools can be identified in the three main basins - Atlantic, Pacific, and Indian (figure 2a). The winter mixed layer encloses the mode water formation pools (see also figure 1). We use a combination of annual minimum PV values and winter (ASO) mixed layer depths to form the horizontal mask for the 'objective function' volume for the suite of adjoint experiments we carry out, whilst ensuring that nothing too close to land or too far north is included. Specifically, we define the objective function as anywhere between 30 and 65°S with a PV value of less than 10^{-13} and an ASO mean MLD (for that given year) of greater than 300m depth, then manually remove regions in the North Pacific and the North Indian Oceans, and close to land around Australia, New Zealand and South America, as we wish to concentrate on the main mode water pools. This mask as calculated for 1999 is shown by the black dotted

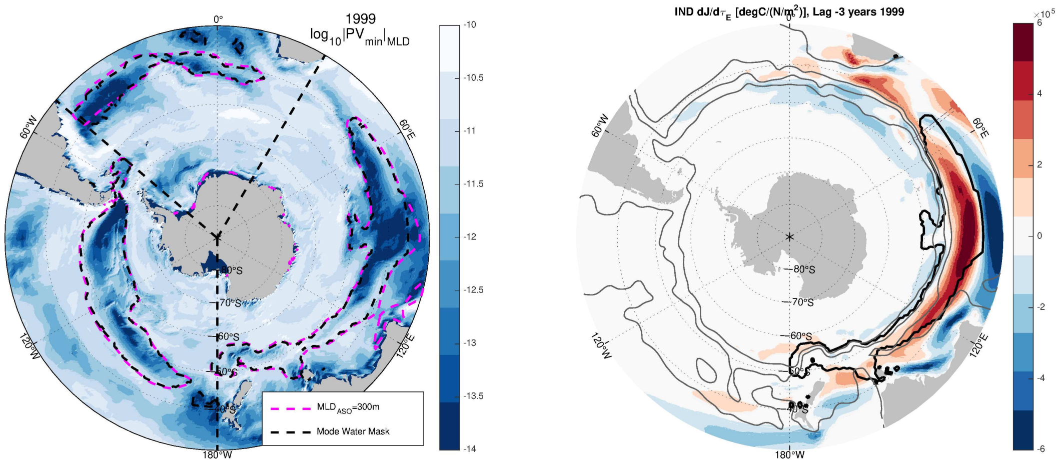

Figure 2. a) The winter mixed layer encloses mode water formation pools laterally: Blue colors are the absolute value (on a $\log_{10}$ scale) of the 1999 minimum PV at the annual mean mixed-layer depth (the green dash-dotted line in figure 1). Also shown are the 300m August-October mean mixed-layer depth contour (pink dotted line) and the extent of the mode water mask (black dotted line), as described further in the text. The domain is also divided into three basins by the three latitudinal black lines shown, into the Atlantic, Indian, and Pacific basins referenced throughout. b) An example sensitivity field: Colors indicate the adjoint sensitivity of the 1999 Indian MWFR heat content to zonal wind stress at approx. 3 years lag. The grey contours indicate the -17, 0, and 30 Sv mean barotropic streamlines, for the entirety of ECCOv4 r2, chosen to highlight the boundary between of the ACC and the sub-tropical gyre structure.

line in figure 2a. The objective function regions are referred to throughout as MWFRs (mode water formation regions).

The climatology of the heat content of the volume of mode water (defined horizontally via the mask and integrated to the depth of the instantaneous mixed layer) for each of the three basins can be seen in figure S1 in the supplementary information. The Indian pool has the largest heat content, followed by the Pacific and Atlantic pools. All three peak in September with a minimum in January or February.

We split the Southern Ocean into three basins using the three latitudinal black dashed lines shown in figure 2a, and calculate a separate objective function for each basin. The Indian and Pacific basins are divided at 180°W, the Pacific and Atlantic at 49.5°W and the Atlantic and Indian at 30.5°E. Because the adjoint model calculates linear sensitivities, the total Southern Ocean sensitivity to a given model variable will be the sum of the sensitivities for each basin, i.e.

$$J_{\mathrm{SO}}^{Y} = J_{\mathrm{Atl}}^{Y} + J_{\mathrm{Pac}}^{Y} + J_{\mathrm{Ind}}^{Y}, \tag{1}$$

where J_b^Y is the objective function in the given basin b in year Y, and thus

$$\frac{\partial J_{\mathrm{SO}}^{Y}}{\partial X}\left(\underline{r}, t\right) = \frac{\partial J_{\mathrm{Atl}}^{Y}}{\partial X} + \frac{\partial J_{\mathrm{Pac}}^{Y}}{\partial X} + \frac{\partial J_{\mathrm{Ind}}^{Y}}{\partial X}, \tag{2}$$

where $\partial J_b^Y / \partial X(\underline{r}, t)$ is the linear adjoint sensitivity of the objective function J_b^Y to model variable X at point $\underline{r} = (x, y, z)$ and time t.

We re-calculate the objective function based on the same MLD and minimum PV criteria for each of the 20 years in ECCOv4 r2. We choose the annual maximum winter mixed layer depth as the vertical extent of our objective function [denoted $\max(\mathrm{MLD}_{\mathrm{ASO}})$].

To capture the peak of the mode water formation, we choose our objective function to extend to the two months on either side of the peak heat contents of the three basin volumes, i.e. from July to November (see figure S1). Thus, our full objective function for a given year and basin is defined as the following volume averaged heat content:

$$J_b^Y = \frac{1}{V_b^Y \Delta t} \int_{\mathrm{Jul}}^{\mathrm{Nov}} \iint^{f_b(x,y)} \int_{z=0}^{\max(\mathrm{MLD_{ASO}})} \rho_0\, c_p\, \theta(\mathrm{r}, t)\, dt\, dxdy\, dz, \tag{3}$$

where $V_b^Y = \iint^{f_b(x,y)} \int_0^{\max(\mathrm{MLD_{ASO}})} dxdy\, dz$ is the control volume in year Y and basin b, Δt is the averaging time interval, $f_b(x, y)$ is the horizontal mask in basin b; ρ_0, a reference density; c_p, the heat capacity of sea water; and θ, the potential temperature. The effect of choosing our objective function as defined above, with the lateral extent limited using our mask, rather than just looking at the entire Southern Ocean mixed layer, is briefly investigated in section A.1.

In order to better understand inter-annual variability and have better statistical behaviour, we carry out an ensemble of adjoint runs, each with objective functions defined in different years. After a number of test runs, we determined that the majority of sensitivity magnitudes had decayed significantly by around 8 years prior to the start of the objective function. Thus we settled on an ensemble of 13 eight-year adjoint runs, with objective functions defined in each winter from 1999 to 2011.

An example sensitivity field, the sensitivity of the 1999 Indian MWFR heat content to zonal wind stress at approximately 3 years lag, can be seen in figure 2b. Thus, red (blue) colors indicate where an increase (decrease) in zonal wind stress in 1996 would result in a linear increase in the Indian MWFR heat content in 1999. The sensitivity has been scaled by $1/\rho_0 c_p$, and thus units indicate the number of degrees C the similarly scaled MWFR heat content would rise if the zonal wind stress changed by 1 N/m^2.

3 Adjoint Results

3.1 Sensitivities to Surface Properties

A range of example ensemble mean sensitivities of the MWFRs to various surface properties can be seen in figure 3, chosen to highlight the range of and main properties of our results. For each ensemble member, sensitivities are output at two week intervals as averages over those two weeks. The sensitivities shown in figure 3 are ensemble averages of winter (July to September) averages, which are then multiplied by a representative scalar standard deviation for the surface property σ_0 (these values can be found in table 1) and scaled by $1/\rho_0 c_p$. This makes the units of sensitivity the amount by which a unit perturbation of the given surface property at the relevant point in space and time would raise the objective function J_b^Y in $^\circ C$. We choose to show winter as it highlights the peak sensitivities (see figure 4 and discussion below). The associated standard deviations (calculated over the ensemble sensitivities) show that ensemble member variation is largely within the magnitude of the sensitivity and not the location of the sensitivity. These standard deviations can be found in the supplementary information, although note that the color scales are not the same as in figure 3.

It should be noted that the adjoint model calculates linearly independent sensitivities, such that the feedbacks between the surface forcings considered here (heat flux, wind stress and fresh water flux) are not included. Thus the sensitivities of the wind stress fields are entirely down to direct wind-driven mechanisms such as Ekman pumping and not by its impact on, for example, net heat flux, and the sensitivities of the net heat flux fields are not influenced by, for example, changes in evaporation rates. This allows for a clean analysis of the sensitivities, whereas the full feedbacks *are* included in forward runs of the non-linear model via bulk formulae, see section 4.

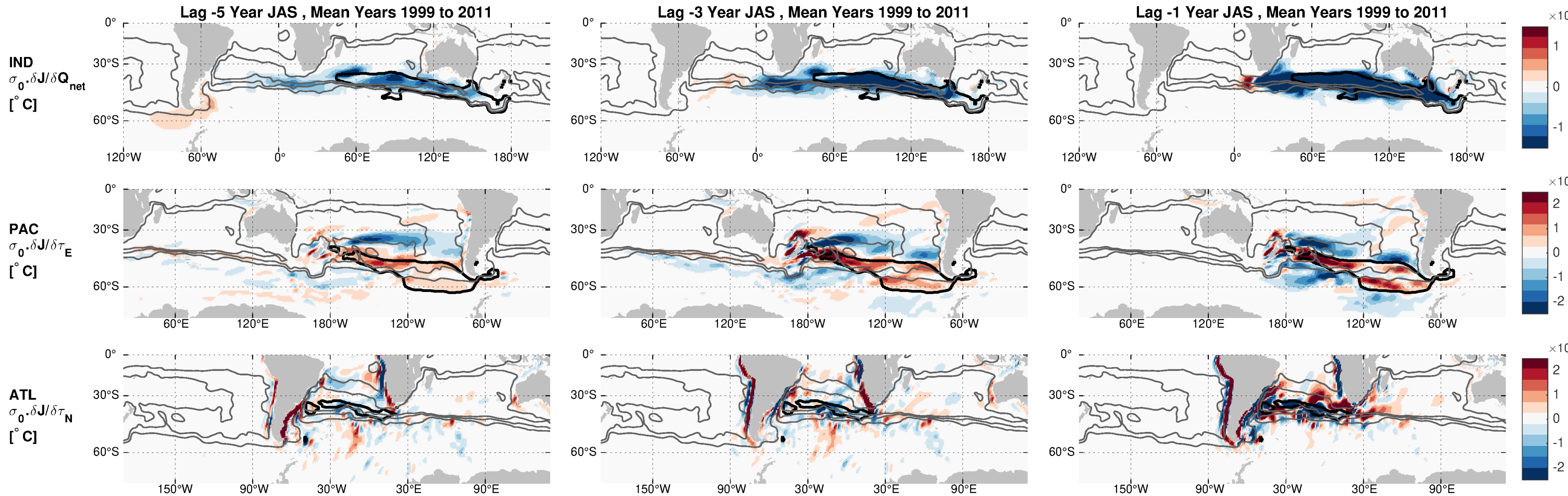

Figure 3. Example sensitivity fields showing the range and general properties of adjoint model simulations: Ensemble mean winter (Jul-Sep) sensitivities for surface properties at lags of 5, 3, and 1 years (left, middle, and right columns respectively). The upper row shows sensitivities of the Indian MWFR (median location indicated by black contour) to surface heat flux Q_{net}. The middle row shows sensitivities of the Pacific MWFR (median location indicated by black contour) to zonal wind stress τ_E. The lower row shows sensitivities of the Atlantic MWFR (median location indicated by black contour) to meridional wind stress τ_N. The grey contours indicate the -17, 0, and 30 Sv mean barotropic streamlines. The associated ensemble standard deviations can be found in the supplementary information.

Table 1. Representative Standard Deviations σ_0 used throughout, calculated from the Southern Ocean mean (S of 30°S) of the ECCOv4 fields' standard deviations.

Property Symbol	Property Name	Standard Deviation
E-P-R	Surface Salt Water Flux	$2.0\text{x}10^{-8}\ \mathrm{m\,s^{-2}}$
Q_{net}	Surface Heat Flux	$60\ \mathrm{W\,m^{-2}}$
τ_E	Zonal Wind Stress	$0.08\ \mathrm{N\,m^{-2}}$
τ_N	Meridional Wind Stress	$0.06\ \mathrm{N\,m^{-2}}$
θ	Potential Temperature	0.3 °C

Q_{net} is defined as positive for heat flux from the ocean to the atmosphere. Thus *negative* sensitivities indicate that a *reduction* in Q_{net}, i.e. *less* heat from ocean to atmosphere, results in an increase in the objective function, i.e. MWFR heat content, and *positive* sensitivities indicate instead that an *increase* in Q_{net} will result in an increase in the objective function. The largely negative sign of the Q_{net} sensitivities (figure 3, upper row) is thus not unexpected, showing that a cooling of the ocean surface in these regions results in a cooling of the MWFR. The location of the peak sensitivity is largely on top of, or at previous lags, "upstream" of the location of the median objective function. Again, this is not unexpected and indicates that simply heating/cooling the source waters for the MWFR results in heating/cooling of the MWFR itself. These features are common across sensitivities to Q_{net} for all lags and in each of the three basins (the Pacific and Atlantic are not shown here), and can be used to identify the source regions of the MWFRs.

The wind stress sensitivities (figure 3, middle and lower rows) have a very different structure to the Q_{net} sensitivities, notably there are significant sensitivities of both signs. Dipole-type structures are common across all such wind stress sensitivities (not just those shown here), with common features including dipoles centered on the boundaries of the objective functions and over source water regions upstream. These types of features we associate with convergence/divergence and thus vertical Ekman pumping/suction of water.

Additionally, the sensitivities to zonal wind stress stretch south across the ACC for all basins, indicating possible links with ACC transport – an increase/decrease in zonal wind stress would imply an increase/decrease in zonal Ekman transport across the ACC. Other common features are what appear to be dynamical links with boundary currents – dynamic because the sensitivities are not in source regions and because the sensitivities often propagate through space over time either along or away from boundaries in patterns similar to topographic, Kelvin, and Rossby waves. This can be seen more easily in the animations provided in the supplementary information and is discussed further in section 3.2.

The negative sensitivity of the Pacific MWFR to zonal wind stress on 1-3 year lags in the region of 120W to 90W and South of 60S (the Amundsen Sea, see figure 3) is consistent with the results of Close et al. (2013), who find a link between an increased Amundsen Sea Low (ASL, resulting in weaker zonal wind stress) and warmer SAMW. However, this sensitivity is relatively weak compared with zonal and meridional wind stress sensitivities over, to the north of, and upstream of the MWFR, whilst Close et al. (2013) believe the ASL is significant in determining SAMW properties. This may be because although the region shows low sensitivity relative to other regions, the actual wind-stress changes in the region are significantly larger than those in other regions. The fact that regions of high sensitivity may not be regions of high variability is discussed further in section 5.3. The lack of a strong cross-ACC link in these sensitivities may also be because the ECCOv4 model has too weak northward transports close to the Antarctic continental shelf, see discussion in Jones et al. (2019a).

The wind stress sensitivities are consistent with the findings of Iudicone, Rodgers, Schopp, and Madec (2007), who find that the export of mode water from the Pacific basin is controlled by the basin-wide meridional pressure gradient – reflected in the basin-wide dipoles in zonal wind stress sensitivities seen here – and by the generation of eastward and westward propagation of Rossby, coastal Kelvin, and equatorial Kelvin waves, also seen here. This suggests that the sensitivity of the export of mode water to the basin-wide pressure gradient (as found by Iudicone et al., 2007) could be related to the sensitivity of the heat content of the mode water in its formation region to the same basin-wide properties (as demonstrated here). In other words, a change in the the zonal wind stress could alter basin-wide pressure gradients, alter the heat content of the mode water, and also lead to, directly or indirectly, changes in the export of that mode water. However, the adjoint model cannot directly represent changes in mixing caused by changes in stratification due to surface flux changes, so this cannot be fully tested in our model.

It should be noted that these are sensitivities of a fixed volume. The sensitivities as calculated cannot indicate whether a warmer mixed layer might shallow and therefore decrease in volume, and thus decrease in overall heat content. This is discussed further in section 4. This may also be why the sensitivities to salinity fluxes are negligible when the influence of salinity fluxes on mode waters has been observed in, for example, Cerovečki et al. (2019); Close et al. (2013). Salinity changes are likely to have a strong influence on the density and therefore volume of mode waters, but not directly on the temperature of our fixed volume MWFRs.

To compare sensitivities between basins and for different variables, we first calculate scaled domain-integrated absolute sensitivities over time for each basin, i.e. the absolute value of the sensitivity is taken before integration, meaning positive and negative sensitivities *do not* cancel out. Thus, the integrated absolute sensitivity is the maximum possible impact on the objective function if perturbations are applied with the same sign and magnitude as the the sensitivities themselves. In each basin, sensitivity to Q_{net} is highest at lag 0 and then decays with a strong seasonal cycle as the lag increases, peaking each winter (figure 4). Here lag 0 is defined as the beginning of the objective function integral, i.e. at the start of July – see (3) – and so non-zero sensitivities are possible at positive lags. Sensitivity to wind stress decays more slowly and has a very slight seasonal cycle, relative to the heat flux sensitivity which it also appears to be out of phase with. The seasonality is determined by the competing seasonal influences of positively and negatively signed regions, see figure 5. Sensitivity to Q_{net} initially dominates in the Pacific basin, with wind stress sensitivity dominating after around 1 year lag. Wind stress sensitivity dominates in the Atlantic basin, and largely dominates in the Indian basin apart from during the objective function integration period (positive lags), where the Q_{net} ensemble mean sensitivity just dominates.

The differences in behaviour between the different basins are likely due to the different locations and sizes of the MWFRs in each basin. The Atlantic MWFR has a relatively small area at the surface and is relatively far north, where it is strongly influenced by the Atlantic sub-tropical gyre and thus wind stress influences are relatively stronger than heat flux. The Pacific and Indian MWFRs both extend over large areas at the surface, but the Indian MWFR has a much larger volume, extending over larger areas than the Pacific MWFR at depth (see figure 6). Thus both the Pacific and Indian MWFRs have strong sensitivity to surface heat fluxes at zero lag, but this is relatively lower than the wind stress sensitivity at larger lags in the Indian ocean, perhaps because the larger volume at depth allows for greater sensitivity to dynamic influences from upstream. Further analysis of the dynamic and kinematic influences on each basin can be found in section 3.2.

These results indicate that the surface heat flux has the largest impact during winter on mode water formed during that same winter, and thereafter seasonally affects subsequent winters, but to a lesser and lesser degree. The large magnitude of the seasonal cycle means that heat fluxes in past winters have a much stronger influence on MWFRs than intervening summers, even years apart. Wind stress, however, can produce a similar or larger impact than heat flux for years to come, with relatively less seasonal variation, perhaps linked to the dynamical, longer-range nature of the connection with the MWFRs. More explicitly, changes in the Ekman pumping over source regions, or changes in ACC strength, or the generation of Rossby waves, could influence the MWFRs for many years, regardless of the local mixed layer depth in the MWFR itself. This is similar to the results of Jones et al. (2019b), who find the heat content of water that subducts from the MWFR is strongly controlled by the sub-tropical gyre strength and structure. This is in turn strongly related to wind-stress over the gyre for the previous 3-4 years.

As well as absolute sensitivities, we also calculate and compare integrated sensitivities with signs intact, and so opposite-signed sensitivities will cancel each other out. We also split the sensitivities by local sensitivities (within the objective function mask), non-local sensitivities (out-with mask), which sum to the total integrated sensitivity. These integrated sensitivities give an indication of the predicted impact on the objective function of a domain-wide positive increase in the surface forcing – this will cause an increase in the objective function due to positive sensitivity regions, and a counteracting decrease due to negative sensitivity regions. The sensitivities in the objective region ('local') are often differently signed to those out-with ('non-local').

The sensitivities to surface fresh water fluxes were calculated, but were found to be of such lower magnitude relative to the Q_{net} and wind stress sensitivities that we did not include them in figures 3,4. For completeness, they are included in figure 5 (upper row). In all three basins, local sensitivities dominate for the first year, peak in magnitude at some point between one and three years lag before decaying away, with a clear seasonal cycle. Local sensitivities continue to dominate in the Atlantic and Indian basins at longer lags, although there is large variability between ensemble members in the Atlantic. In the Pacific basin, non-local sensitivities dominate at lags greater than one year, and do not appear to be decaying significantly after eight years of lag, although again there is relatively large variability. There is a clear seasonal cycle apparent in all sensitivities. Thus, local sensitivities to fresh water forcing are important at timescales of up to three years, and non-local sensitivities can remain relatively large, but with large variability between basins and ensemble members.

The sensitivities to Q_{net} (figure 5, second row), being largely single-signed, show very similar behaviour to that in figure 4, with a pronounced seasonal cycle and strong decay over time. The local sensitivity dominates for the first year or two in all basins, before the non-local begins dominate in the Atlantic and Pacific basins. However, the local sensitivity continues to dominate at longer lags in the Indian basin, likely because the Indian MWFR has the largest volume, see figure S1 in the supplementary information.

For sensitivities to both zonal and meridional wind stress (figure 5, third and fourth rows), the local sensitivity in each basin dominates for one year (Atlantic and Pacific basins), or not at all in the Indian basin. The local and non-local sensitivities are largely of opposite sign, related to the dipole structures seen in figure 3. There is also a larger seasonal cycle apparent, especially in the sensitivities to zonal wind stress τ_E, with local and non-local sensitivities being out of phase with each other. This suggests the seasonal influences on positive and negative sensitivities cancel each other out when the absolute sensitivity is calculated, leading to the much smaller seasonal cycle when looking at the absolute sensitivities in figure 4.

The time dependence of the sensitivity to heat fluxes suggests a process very much dominated by mixed layer properties - the sensitivity is largest in the winter when mixed layers are deepest, and information about past years is lost over time, with sensitivities at two years lag around half of that at zero years. This is consistent with the fields in figure 3 that show sensitivities confined to the objective function region (where the mixed layers are deepest) and upstream. The slower decay and relatively weaker seasonal cycle in the wind stress sensitivities also point to the influence of more dynamical processes, which are not strongly linked to local mixed layer depths and have stronger influences at larger lags.

The seasonal basin-wide mean mixed layer depths (means within each basin south of 30°S) correlate tightly with the Q_{net} sensitivity seasonal cycles in all basins, in all years, in all ensembles (max R^2 within ensemble members = 0.98–0.99). They also correlate well with the seasonal cycle of the mean wind stress sensitivities in the Indian basin (ensemble max R^2 =0.87–0.97). Looking at ensemble member to ensemble member variability in peak sensitivities, the link with mixed layer properties is less clear. There is a statistically significant, but weak ($R^2 = 0.33$) correlation between the annual maximum of the whole Southern Ocean mean MLD (south of 30°S) and the ensemble member peaks in total Q_{net} sensitivity (summed over the three basins), but not for individual basins. In the Indian basin, there are statistically significant correlations between ensemble member peak absolute wind stress sensitivities and the annual maximum Indian ocean mean MLD ($R^2 = 0.55/0.68$ for $\tau_{N/E}$).

These correlations imply the seasonal variation in Q_{net} sensitivities are almost entirely controlled by the mixed layer, but that year to year changes in peak sensitivities are not so clearly related to mixed layer properties. We speculate that this could be because year to year changes integrate influences over many years, so that the relationship with individual years is not as clear. Conversely, whilst the Atlantic and Pacific wind stress sensitivities are not strongly correlated with mixed layer properties on seasonal and inter-annual timescales, the Indian basin wind stress sensitivities show a link with mixed layer properties on both timescales, although it is the mean sensitivity that shows seasonal links, and the absolute sensitivity that shows inter-annual links. The mean wind stress sensitivities show a more pronounced seasonal cycle than the absolute, ccf figures 4 and 5, showing that the overall sensitivity to a domain-wide single-sign increase in wind stress is controlled by mixed layer properties on a seasonal time-scale. However, on an inter-annual time-scale, it is the absolute sensitivity that is partially controlled by peak mixed layer depths.

3.2 Sensitivities to Kinematic and Dynamic Potential Temperature

As in Marotzke et al. (1999) and Jones et al. (2018), we analyze the sensitivities of the objective function to potential temperature by splitting it into sensitivities due to changes in temperature along isopycnals (referred to as kinematic changes) and changes in temperature that result in density changes (referred to as dynamic changes).[1] This

[1] The definition of kinematic and dynamic changes may remind the reader of ‘spice’ and ‘heave’. These are most often used to refer to the decomposition of temperature changes in time at a fixed depth into changes on neutral density surfaces (spice) and changes due to the motion of these surfaces (heave)(see, for example Bindoff & Mcdougall, 1994). Whilst this decomposition is conceptually similar, the definitions are different from our decomposition here. We are considering the changes in our objective function J, a non-trivial function of temperature, at constant salinity. Kinematic anomalies are possible changes in potential temperature at a fixed density at one point in time, which is not quite the same as ‘spice’ anomalies, normally defined as a change over time of potential temperature at a fixed density. Dynamic anomalies are related to changes in density at fixed salinity, which is similar to but not the same as ‘heave’, related to the change in the height of a density surface over time.

is achieved by considering our objective function as a function of both density and potential temperature, i.e. $J = J[\rho(\theta, S), \theta]$, where ρ is density and S is salinity. Thus the sensitivity to potential temperature can be written

$$\left(\frac{\partial J}{\partial \theta}\right)_S = \left(\frac{\partial J}{\partial \rho}\right)_\theta \left(\frac{\partial \rho}{\partial \theta}\right)_S + \left(\frac{\partial J}{\partial \theta}\right)_\rho, \tag{4}$$

where the first term on the RHS is identified as the dynamic component of the sensitivity, and the second term the kinematic. We then use the definitions of the of the coefficients of thermal expansion α and of haline contraction β:

$$\alpha \equiv -\frac{1}{\rho}\left(\frac{\partial \rho}{\partial \theta}\right)_S \text{ and } \beta \equiv \frac{1}{\rho}\left(\frac{\partial \rho}{\partial S}\right)_\theta, \tag{5}$$

to write

$$\left(\frac{\partial J}{\partial S}\right)_\theta = \left(\frac{\partial J}{\partial \rho}\right)_\theta \left(\frac{\partial \rho}{\partial S}\right)_\theta = \beta\rho\left(\frac{\partial J}{\partial \rho}\right)_\theta, \tag{6}$$

and so the dynamic sensitivity can be written:

$$F_{\text{dyn}} = \left(\frac{\partial J}{\partial \rho}\right)_\theta \left(\frac{\partial \rho}{\partial \theta}\right)_S = -\frac{\alpha}{\beta}\left(\frac{\partial J}{\partial S}\right)_\theta. \tag{7}$$

Then, rearranging (4) we can write the kinematic sensitivity as:

$$F_{\text{kin}} = \left(\frac{\partial J}{\partial \theta}\right)_S + \frac{\alpha}{\beta}\left(\frac{\partial J}{\partial S}\right)_\theta. \tag{8}$$

Thus we can calculate both dynamic and kinematic sensitivities from the sensitivities to potential temperature and salinity [$(\partial J/\partial\theta)_S$ and $(\partial J/\partial S)_\theta$] output directly from the MITgcm adjoint model in combination with the factor α/β calculated from the model output potential temperature on the same two week average time-steps using the TEOS-10 toolbox (McDougall & Barker, 2011). Note that, unlike the sensitivities to surface fields, each dynamic/kinematic sensitivity snapshot is a three-dimensional field that also depends on depth.

We calculate ensemble mean dynamic and kinematic sensitivities for the same experiments as previously discussed, where the objective function is the heat content of MWFRs. The sensitivities are scaled by $1/\rho_0 c_p$ and so are unitless, i.e. the amount by which the objective function would increase in $°C$ for a dynamic/kinematic rise in potential temperature of $1°C$.

The ensemble mean dynamic sensitivities at 4 years lag and 442m depth have significant distinct single-signed regions of both signs, as well as dipoles (figure 6a, other lags and shallower depths are similar, but at longer/shorter lags extend further/less far [not shown]). Positive dynamic sensitivity indicates that decreasing the density (deepening the density surfaces) at this point would result in an increase in the MWFR heat content, and conversely negative dynamic sensitivity indicates increasing the density (raising the density surfaces) would result in an increase in the MWFR heat content. Within the objective function volume (indicated by the black contours) the sensitivity is largely positive, implying downwelling will produce an increase in the MWFR heat content. As can be seen with comparison with figure 6b, much of the strong dynamic sensitivity is placed along the same location as source waters, indicated by strong kinematic sensitivities, but they also stretch further south across the ACC. In the Indian sector, as in the Pacific sector, there are dynamic sensitivities of both signs, both over source regions and extended around these regions. These can be interpreted as highlighting that changes in the strength and structure of the ACC and sub-tropical gyres can draw more or less heat into the mixed layer.

The dynamic sensitivity of the Atlantic sector shows a strong dipole directly in the region of the objective function - although 443m is below the median depth of the objective function, the structure of sensitivities is similar at shallower depths. This pattern rotates in place over time in an anti-clockwise or cyclonic direction, consistent with the westward motion of sensitivity peaks centered at $\sim$30°S and the eastward motion of sensitivity peaks at $\sim$40°S. This is another indication that the ECCO Atlantic mode water pool is strongly controlled by the dynamics of the Atlantic sub-tropical gyre.

In general, dynamic sensitivities for all three sectors are a mix of positive and negative regions, with strong links to topographic features. Viewed as animations, one can see that there are many dynamical features that are generated at topographic boundaries and then propagate along or away from these boundaries in behaviour that resembles that of Kelvin, Rossby, and topographic waves. Some animations can be viewed in the supplementary information.

The mean kinematic sensitivities at 4 years lag and 442m depth, by contrast, are largely single signed (figure 6b, sensitivities at shallower depths and at longer/shorter lags are very similar but extend further/less far upstream [not shown]). The Indian and Pacific pools, being close to the northern ACC boundary, are affected by kinematic temperature changes upstream in the ACC, stretching around half its path at 4 years lag. Conversely, the Atlantic pool is shallower and further north, more firmly in the sub-tropical gyre, and as such is highly sensitive to local gyre kinematic temperature changes rather than changes in the ACC. As kinematic temperature changes take place on isopycnals, the sensitivities strongly resemble a passive tracer sensitivity and so reflect the influences of direct heat fluxes or irreversible mixing. In fact, one can directly calculate passive tracer sensitivities in the adjoint model, and they are highly correlated with the kinematic sensitivities at the depths of the objective function (see figure in supplementary information). As we consider longer timescales, kinematic sensitivities weaken and are found further away along source paths.

Similarly to section 3.1, we can calculate the domain-integrated dynamic and kinematic sensitivities for each basin, and split the integrals into local (within objective function volume) and non-local (out-with objective function volume), which sum to the total integrated sensitivity.

The dynamic sensitivities are generally of an order of magnitude smaller than the kinematic sensitivities (figure 7). The local dynamic sensitivities are all positive and peak within two years, decaying with time after. The non-local dynamic sensitivities all begin negative (indicative of the dipole structures seen throughout the dynamic sensitivity fields, see figure6b), but then largely become positive and grow with increasing lag (although there is significant within ensemble variability). The Indian non-local sensitivity is still growing at 8 years lag, with the Pacific looking like the ensemble mean may have peaked and the Atlantic sensitivity unclear.

The local kinematic sensitivities peak at 0 lag then quickly decay, and the non-local sensitivity takes over as the tracer-like sensitivity moves upstream. The local sensitivities decay with e-folding timescales of roughly 14, 15, and 18 months for the Atlantic, Pacific and Indian basins respectively, then reach a steady minimum after 4, 5, and 8 years. The difference in timescales can be attributed to the size of the MWFRs – the mean heat contents of the MWFRs increase as the timescales increase, i.e. the Atlantic is the smallest MWFR and the Indian is the largest, see figure S1 in the supplementary information. The total and non-local sensitivities appear to reach a peak value at around 2 years lag and to still be slowly decaying at 8 years lag.

4 Perturbation Experiments

Adjoint sensitivities, such as those presented in section 3, are predictions about the sensitivity of the objective functions - in our case the heat content of fixed volumes - in an adjoint linear model. Thus, we expect them to predict the linear aspect of the equivalent perturbation experiments in the full non-linear model. They are considered most useful when investigating quantities that can be expected to behave linearly, such as integrals over relatively large volumes and/or time spans. As discussed in section 1, we consider adjoint sensitivities to be a useful tool for discovering which regions and timescales are of interest, but not a replacement for fully non-linear experiments. In this section, we use the adjoint sensitivities from section 3 as a starting point for a series of perturbation experiments which we use to directly investigate the impact of changes in surface forcings on our objective function, including assessing the degree of linearity in the responses, i.e. the impact of dynamics not captured in the adjoint model.

An additional complication to comparing the linear adjoint sensitivities with non-linear perturbation studies comes from the bulk formulae used in MITgcm. Whilst the adjoint model produces linearly independent sensitivities for the model surface forcings considered, perturbing the same forcings in the full model can change many different aspects of air-sea heat and momentum exchange. For example, a change in ocean heat flux produces a related change in evaporation rates, and a change in wind stress produces a related change in heat flux, neither of which are accounted for in the adjoint sensitivity fields. Whilst it would be possible to alter the model code in order to perturb these variables separately, the action of the bulk formulae is to produce more realistic perturbations, as in the real ocean no such independent changes would occur. Additionally, as discussed, the non-linear forward model is expected to behave differently than the adjoint linear model; this is merely one of many factors causing them to differ, and it is informative to see the full difference between the two models.

In the results that follow, we follow Verdy et al. (2014) and use the combination of oppositely signed perturbation experiments to decompose the linear and non-linear responses. This allows for qualitative and quantitative analysis of the two different types of effect, and allows us to test our assumption that the non-linear component of our objective function is small compared with the linear. Further details of the derivation of the linear and non-linear responses can be found in A.2. We investigate perturbations in the surface heat flux and the zonal and meridional wind stresses, applying these in regions where sensitivities are relatively high. We also include a test case where strong perturbations are applied to an unresponsive region, as defined by low adjoint sensitivities.

4.1 Q_{net} Pacific Perturbation

For our first perturbation experiment, we chose a region in the South-East Pacific identified in other studies as important for downstream Sub-Antarctic Mode Water (SAMW) properties (Naveira Garabato, Jullion, Stevens, Heywood, & King, 2009), and additionally which shows an interesting pattern of heat flux sensitivity. At two years lag, the Atlantic MWFR has a region of positive sensitivity in this region of the South-East Pacific, just upstream of Drake Passage (see figure 8a upper panel). This implies that positive heat flux perturbations in this region i.e. increasing heat loss to the atmosphere, will result in a warmer MWFR in the Atlantic in 2 years time (as previously stated, Q_{net} is defined as positive out of the ocean). Notably there is negative sensitivity over the region of the objective function, so increasing heat loss directly over the Atlantic MWFR would result in a *cooler* MWFR in 2 years time.

We designed a set of four perturbation experiments to test the sensitivity of the forward nonlinear model to changes in net heat flux in this key region. The black dashed contours in figure 8a show the region over which the Q_{net} perturbations were applied, in four separate step changes with magnitudes of ± 10 Wm^{-2} and ± 100 Wm^{-2}, constant over the box indicated. These perturbations were applied to the forward non-linear ECCOv4 r2 model at the beginning of the model run. Additionally to the changes in $Q_{\rm net}$, there were resultant changes in the salt flux E-P-R, which we do not show because, as demonstrated in section 3, the sensitivities to this flux are extremely low. Thus the resultant experiment is close to being a test of the influence of $Q_{\rm net}$ independent of other surface fluxes. The perturbation region has a mean $Q_{\rm net}$ of 20 W/m^2 and a seasonal cycle of amplitude 120 W/m^2 in ECCOv4 r2, and so the ± 10 Wm^{-2} perturbations are of similar magnitude to the mean, whereas the ± 100 Wm^{-2} perturbations completely alter the entire seasonal cycle, shifting the region to entirely positive values year-round, or else largely negative.

The perturbation region sits over the Pacific MWFR (see figure 8a, middle panel), where the sensitivity is large and negative, showing that increasing the heat flux from ocean to atmosphere is an efficient way of cooling this region. At 5 years lag, the Indian MWFR shows weak positive sensitivity to $Q_{\rm net}$ in the perturbation region (figure 8a, lower panel). Thus, for a positively-signed $Q_{\rm net}$ perturbation in the region indicated, we expect the Atlantic objective function to show a linear increase in heat content after roughly 2 years, we expect an instantaneous strong decrease in heat content in the Pacific objective function, and after roughly 5 years we expect an increase in heat content in the Indian objective function.

We calculate the integrated heat content of the objective function regions for all four perturbation experiments, which is integrated to the fixed maximum winter MLD, following the definition of the objective function J_b^Y:

$$\text{fix}H_b^Y(\theta, t) = \iint^{f_b(x,y)} \int_{z=0}^{\max(\text{MLD}_{\text{ASO}})} \rho_0\, c_p\, \theta(\text{r}, t)\, dxdy\, dz, \tag{9}$$

and thus the change in heat content with respect to the control simulation (the standard ECCOv4 r2 solution)

$$\Delta\text{fix}H_b^Y(t) = \text{fix}H_b^Y(\theta' - \theta, t), \tag{10}$$

where θ' is the perturbed simulation potential temperature field and θ is that from the control simulation. The MLD is taken from the control simulation and is therefore the same depth as used in the objective function for the adjoint sensitivity experiments. We also calculate the heat content of the mode water formation regions calculated using the objective function mask for that year, $f_b(x, y)$, but the time-varying *instantaneous* mixed layer depth in each of the perturbation simulations:

$$\text{var}H_b^Y(\theta, t) = \iint^{f_b(x,y)} \int_{z=0}^{\text{MLD}(t)} \rho_0\, c_p\, \theta(\text{r}, t)\, dxdy\, dz, \tag{11}$$

and thus the change in the varying-volume heat content

$$\Delta\text{var}H_b^Y(t) = \text{var}H_b^Y(\theta' - \theta, t),\ \text{MLD} = \text{MLD}'(t), \tag{12}$$

where the MLD is taken instantaneously from the perturbed simulation. To differentiate between the two volumes, the fixed-volume of the objective function and the instantaneously calculated, varying volume mode water formation region, we refer to them henceforth as the fix-MWFR and var-MWFR, respectively.

We combine the results of the positively and negatively signed experiments to produce the linear and non-linear impacts for the ± 10 Wm^{-2} and ± 100 Wm^{-2} perturbations. We choose the combinations such that the sign of the linear/non-linear changes indicate the changes for the positively signed $Q_{\rm net}$ perturbations. Note that the heat content changes are discontinuous at the year boundaries due to the changing objective function definition for each year, as the objective function is based on the PV and MLD properties for every individual year, as discussed in section 2. The magnitude of the changes can be significantly larger for the varying-volume heat contents than the fixed-volumes as the changes in the volume due to changes in the instantaneous MLD result in much larger heat content changes than potential temperature changes alone (see figures 8b and c, noting the different y-axis scales.)

One would expect the normalized linear response to be identical for both magnitudes, by definition, and this is largely true, especially for the fixed-volume heat content (see figure 8b, thick lines, which lie mostly on top of each other). There are small differences at the peaks of the varying-volume responses, likely due to the fact that the bulk formulae effects discussed previously will have introduced some non-linear changes to the perturbations that will result in the positive- and negative-signed experiments not being exactly symmetric. The non-linear effects (figure 8b and c, thin lines) are smaller in general than the linear effects, but increase in the ± 100 Wm^{-2} case (red lines), as would be expected, becoming almost as large as the linear changes, especially in the Atlantic.

The predicted positive response is seen in the Atlantic (figure 8b and c, upper panels), with both the fix-MWFR and var-MWFR showing linear increases in heat content, starting after roughly 2 years. The heat content of the var-MWFR (figure 8c) shows large spikes every winter as the mixed layer deepens, but largely agree with the sign of the heat content change of the fix-MWFR (figure 8b).

In the Pacific, at all lags a negative response is expected, and this is borne out in the fix-MWFR heat content changes (figure 8b middle panel). However, the sign of the linear change in the var-MWFR (figure 8c middle panel, bold lines) is opposite to that of the fix-MWFR: when the heat flux to the atmosphere increases, as in the +10 and +100 Wm^{-2} experiments, the temperature in the fix-MWFR decreases and so does the heat content, but the heat content of the var-MWFR *increases*. This is because the cooler mixed layer deepens, resulting in more net heat content, as can be seen in figure 9.

The responses the Indian region (figure 8b lower panel) are consistent with simple advection downstream - it takes over three years for the effect of the perturbation to reach the Indian region, and it remains much lower magnitude than either the Pacific or Atlantic effects. After this, the impact grows year on year, and similarly to the Pacific basin has an opposite-signed linear effect on the fix-MWFR and the var-MWFR. Like the Atlantic, an increase in heat loss to the atmosphere results in an overall warming of the fix-MWFR, and vice-versa. The opposite sign of the response of the fixed and varying volume heat contents is for the same reason as in the Pacific, namely that a warming mixed layer shallows and so decreases its overall heat content when the volume considered is allowed to evolve.

Whilst the fix-MWFRs do indeed warm or cool as expected, these lead to changes in MLD that act counter to the temperature change and result in a larger mixed layer heat content when the mixed layer cools and a lower mixed layer heat content when the mixed layer warms (figure 9). Whilst the temperature change is very linear, the change in MLD has a significant non-linear component, although the linear component is still largest. This is not surprising as the temperature response is strongly linked with the imposed linear Q_{net} changes, whereas the mixed layer response is, as the name suggests, mediated by mixing, a non-linear process.

These results demonstrate that the adjoint sensitivities can indeed successfully predict the linear sensitivity of the fix-MWFRs in forward, non-linear simulations. However, these results also highlight that the var-MWFRs, calculated instantaneously, do not necessarily respond in the same manner as their fixed-volume counterparts. In fact the var-MWFRs seasonally respond with higher magnitudes than the fix-MWFRs. Whilst the sign may not be predicted, the fact that the heat content does significantly change is predicted. Additionally, as might be expected, larger magnitude perturbations lead to slightly larger normalized non-linear effects.

4.2 τ_E Pacific Perturbation

We now consider a regional experiment perturbing the zonal wind stress, τ_E. In winter and at three years lag, a clear dipole in the ensemble mean sensitivity of the Pacific MWFR to τ_E can be seen stretching east from New Zealand well into the Pacific (figure 11, middle panel). This indicates that a zonal wind stress dipole of this sort, implying downwelling along the dipole center, would produce an increase in the heat content of the objective function region (median location indicated by the black contours). A perturbation closely matching this dipole was chosen to test this sensitivity (figure 10, black contours) which was applied either as indicated, with two oppositely signed regions of magnitudes ± 1 Nm^{-2}, or with the signs of the two regions reversed. These two perturbations were applied separately as step changes to the forward non-linear ECCOv4 r2 model at the beginning of the model run (the start of 1992). These are large magnitude shifts, as the mean dipole amplitude is $\sim$1 Nm^{-2}, with a seasonal amplitude also $\sim$1 Nm^{-2}, in ECCOv4 r2. This is intended to push the linear assumptions to the limits, by testing perturbations the same order of magnitude as the climatological means.

Additional to the changes in τ_E, there were resultant linear and non-linear changes in the heat flux Q_{net} (figure 10, color). The consistent non-linear impact of the τ_E forcing of both signs is to decrease the ocean-atmosphere heat flux Q_{net}, i.e. an increase in wind stress of any sign results in a surface warming. There is also a smaller magnitude linear component with a more complicated structure.

We now look at the relative importance of the linear and non-linear contributions on both the fix-MWFR and var-MWFRs, the latter calculated as before from the lateral extent of the objective functions but integrated in depth to the instantaneous MLD (figures 11b and c). The fix-MWFR heat content in the Pacific and Indian sectors responds linearly (figure 11b, blue lines) with an increase that grows over time, as predicted by the sensitivities in the perturbation regions indicated in the left hand panels. The non-linear responses (red lines) initially grows with the opposite sign, but after 3-5 years are relatively close to zero again.

Conversely, the var-MWFR heat contents (figure 11c) also grow over time, but both linear and non-linear components remain very similar, apart from seasonally during winter in most years. This reflects the fact that the negatively signed perturbation has a limited impact on the var-MWFR heat content, and so the linear and non-linear components are both dominated by the positive perturbation response, apart from in winter. This is likely due to the linear response to the wind stress perturbation competing with the response to the non-linear heat flux forcing, i.e. the negatively signed wind stress perturbation and the non-linear heat flux anomaly result in opposing influences on the varying-volume heat content of similar magnitudes. This can be seen clearly for the Pacific sector comparing the nonlinear Q_{net} anomalies (figure 10) with the Q_{net} sensitivity of the Pacific MWFR (figure 8, middle left panel) – the large negatively signed nonlinear Q_{net} anomaly sits partially over the region of large negative Q_{net} sensitivity and thus acts to increase the heat content of the Pacific MWFR in both the positively- and negatively-signed τ_E perturbations. This also alters the fix-MWFR heat contents, but the positive impact from the Q_{net} sensitivity is much smaller as it is not amplified by the accompanying volume change as in the var-MWFR changes.

In the Atlantic sector, both the linear and non-linear fix-MWFR responses show relatively little response (figure 11b, noting the different limits of the y-axes, which are two orders of magnitude lower for the Atlantic). The var-MWFR responses (figure 11c), similarly to the Pacific and Indian sectors are practically identical for the linear and non-linear components, but unlike the Pacific and Indian sectors, do not show any seasonal differences, as the var-MWFR response is effectively zero at all times for the negatively-signed perturbation.

These results show that, again, the adjoint sensitivities can accurately predict the linear response of the fix-MWFRs, with a relatively low non-linear response, especially at longer timescales. However, due largely to the non-linear Q_{net} perturbations shown in figure 10, the response of the more realistic var-MWFR is much more non-linear. Interestingly, the degree of non-linearity varies seasonally in the Pacific and Indian pools, where the responses are larger in general. This suggests that, whilst the large non-linear effects cannot be ignored, they may be seasonally unimportant, namely during winter when the MWFR is largest. Thus the adjoint sensitivities are most accurate, and therefore most useful, for looking at sensitivities when the linear response is large. Linear responses are large when looking at individual winter-time peaks, and multi-year averages will also be dominated by the winter contributions and therefore largely linear. This confirms that the adjoint sensitivities are most useful for predicting relatively long term averages and are not always suitable for looking at seasonal or shorter timescales.

4.3 τ_N Indian Ocean perturbation

The results of sections 4.1 and 4.2 confirm that the adjoint sensitivities can predict regions of objective function sensitivity in the full non-linear model. We now demonstrate the corollary, namely that perturbations in regions with low adjoint sensitivities produce weak responses in the full non-linear model.

A region east of Africa in the Indian ocean, which is a region of low adjoint sensitivity for both heat flux and wind stress at any time scale modeled, was chosen to test this sensitivity (figure 12, black dashed contour). This step change perturbation was applied either as indicated, or with the opposite sign, i.e. magnitudes ± 1 Nm^{-2}, one to two orders of magnitude larger than the ECCOv4 r2 mean and seasonal cycle amplitude (0.03 and 0.06 Nm^{-2}, respectively) for this region. These two perturbations were applied separately as step changes to the forward non-linear ECCOv4 r2 model at the beginning of the model run (the start of 1992). Additionally to the changes in τ_N, as in section 4.2 there were resultant changes in the heat flux Q_{net}. Whilst there are significant linear effects (figure 12, LH panels), the non-linear effects are extremely large (RH panels), on the order of 100 Wm^{-2}.

Figures 13a and b show the derived linear/non-linear responses of the fix-MWFR and var-MWFR heat contents respectively, derived as before. All basins show linear and non-linear effects of similar magnitudes, apart from the fix-MWFR non-linear impact in the Indian sector (red line, bottom panel) being significantly larger than the linear response (blue line). It should be noted that the order of magnitude of the heat contents displayed here are an order of magnitude less than those depicted in figure 11.

These results confirm that perturbing regions with low adjoint sensitivity produces weak linear responses (when compared with regions of significant sensitivity). Of course, this does not result in no linear response whatsoever in the objective function region, just that it is relatively small and of similar magnitude to the non-linear response. The responses, including the non-linear component, are at least an order of magnitude lower than those found in section 4.3, especially relevant when the magnitude of the anomaly is so large.

5 Summary and Discussion

We have identified the location of winter mode water formation pools within the mixed layer of an observationally constrained model of the Southern Ocean (Forget et al., 2015). Using an adjoint model, we have determined the sensitivity of the fixed-volume heat contents of these mode water formation regions (MWFRs) to surface forcings, changes of potential temperature at constant density, and changes of potential temperature that lead to changes in density, in an ensemble of 11 eight year simulations. These determine the sensitivity of the winter heat content of the MWFRs in the years 1999 to 2011 to the properties mentioned in previous years. We have highlighted the key aspects of the sensitivities here, with further results available in the supplementary information.

5.1 Summary of Sensitivity Results

Analysis of the sensitivity fields revealed that, on the eight year time scale investigated in our adjoint model, the heat content of the MWFRs is significantly affected by surface net heat fluxes and wind stress, but not by fresh water fluxes (discussed further on), see section 3.1 for further details. The heat content of MWFRs was found to be most sensitive to local (within the MWFR), recent (within the last year) changes to surface heat fluxes. There were also significant sensitivities to non-local (outside the MWFR) wind stress changes from 2-8 years previously. The locations of the sensitivities in previous years were similar across ensemble members, with the variability between ensemble members largely in the magnitude of the sensitivities, rather than the sign.

Heat flux sensitivities were largely single-signed, indicating a link between increased ocean to atmosphere heat fluxes and decreased heat contents in MWFRs, and vice-versa. At longer lags, the location of the sensitivities moved upstream, indicating the source water regions and subsequent advection pathways for the MWFRs. Sensitivities at any given location, as well as the domain-integrated sensitivities, decreased in magnitude with time. There was a strong seasonal cycle, with the largest sensitivities occurring during previous winters, with strong correlations with the mixed layer depth seasonal cycle. This implies that surface heat fluxes are most effective at changing the heat content of MWFRs during winter, when the heat content throughout the deepened mixed layers can be influenced. The mixed layer has a 'memory' that allows for changes in one year to affect heat content the next year, indicated by the significant sensitivities in previous winters, although there is a clear decay with time that indicates the influence drops year by year, and is largely limited to changes within the last four to six years. This extends the role of SAMW formation preconditioning discussed in Sloyan et al. (2010) beyond a single season and over several years. It also aligns well with recent results looking at SAMW variability in the Pacific (Cerovečki et al., 2019; Meijers, Cerovečki, King, & Tamsitt, submitted) who find that while inter-annual variability in SAMW properties is largely the result of local instantaneous forcing, preconditioning from upstream waters also influences properties on lags of 1-2 years.

Wind stress sensitivity patterns largely resembled dipole patterns, and show a less pronounced decay in magnitude with time and a less pronounced seasonal dependence (when compared with the heat flux sensitivities), although the largest MWFR, in the Indian basin, showed a seasonal dependence between mean wind stress sensitivities and mixed layer depths. Dipoles were found centered over the MWFRs or their source regions, indicating the importance of vertical Ekman pumping/suction to modifying the heat content. Dipoles of similar magnitude were also observed over the sub-tropical gyres and along topographic features, implying that wind stress changes can change the heat content of MWFRs effectively through dynamical processes, such as altering the strength of the gyre circulations, or by generating Rossby, Kelvin, or topographic waves. The zonal wind stress sensitivities also extend significantly farther south than for other properties, indicating a link with ACC dynamics. This is consistent with the findings of Rintoul and England (2002), who find that Ekman transport across the South Antarctic Front (SAF) south of Australia (at roughly 50S) is responsible for the variability in T and S properties of SAMW (Sub-Antarctic Mode Water) in this region, rather than the variation of surface fluxes.

The lack of stronger sensitivities to wind stress or heat fluxes south of the ACC could be interpreted in a number of ways. The first is that the ECCOv4 model fails to accurately represent the processes responsible for these links in observations, with, for example, too weak off-shelf transport rates. The second is that the regions of high variability in observations are not co-located with regions of high sensitivity. Investigating how observed variance might look when convolved with our sensitivities is part of our planned future work, see section 5.3. A third possibility is that the processes that bring strong influences from south of the ACC into the mode water regions are largely non-linear, and thus the linear sensitivities do not reveal them, although they may be present in forward fully non-linear simulations.

Finally, it may be that the influence of the waters from south of the ACC on the MWFRs is largely on the volume of the mode water pool, which is not something our sensitivities are designed to show. This would be consistent with the results of, e.g., Gao, Rintoul, and Yu (2018) who find wind stress curl changes lead to deepening or shoaling of the base of the winter mixed layer, and subsequently influences the volume of SAMW formed. Additionally, Meijers et al. (submitted) find that the Pacific SAMW volume is strongly controlled by local wind stress and heat fluxes poleward of 55°S, whereas the mean temperature is not strongly linked to local surface forcings, implying it is set by advection from upstream, consistent with our results.

The analysis of sensitivities to surface forcings was supplemented by analysis of the sensitivity of the heat content of MWFRs to potential temperature, split into kinematic (at constant density) and dynamic (involving changes in density) components. Kinematic sensitivities were largely single-signed positive, strongly resembled passive tracer sensitivities and thus were largest in direct source regions for the MWFRs. Dynamic sensitivities showed both signs and indicated the effects of raising/lowering density surfaces. A summary of the results can be seen in figure 14. The largest sensitivities were over source regions as well as along topographic features, across the Southern ACC, and in the subtropical gyres. This

5.2 Summary of Perturbation Experiments

Given that the adjoint model is strictly linear, we chose a small set of perturbation experiments to test the validity of these results in the full forward non-linear model. We chose regions highlighted by previous studies to be of relevance for mode water properties that were also highlighted by the sensitivity fields. We deliberately chose large (compared with the climatological mean) perturbations in surface forcings to show the limits of the linear behaviour.

The first perturbation experiment was a step change of the ocean-atmosphere net heat flux in the South-East Pacific, just upstream of Drake Passage. This is identified in Naveira Garabato et al. (2009) as a region where wintertime heat fluxes influence the properties of Drake Passage SAMW. Additionally, our adjoint experiments identify it as a region where the Pacific MWFR heat content is negatively sensitive to increases in ocean-atmosphere fluxes on short timescales, and where Atlantic MWFR heat content is *positively* sensitive on timescales of two years or more. The Pacific region sensitivities support the conclusions of Naveira Garabato et al. (2009): the sensitivities indicate that changing heat fluxes upstream of Drake Passage directly influences the heat content of the Pacific MWFR, water which then travels into Drake Passage as SAMW where it is measured by the repeat transects used in Naveira Garabato et al. (2009).

The results of the Pacific heat flux perturbation experiment confirmed the expected linear decrease in the heat content of the fixed-volume MWFR in the Pacific region when the heat flux from ocean to atmosphere was increased upstream of Drake Passage. We also saw the expected linear increases in heat content in the Atlantic and Indian fixed volume MWFRs as predicted by the adjoint sensitivities. The non-linear changes in the fixed-volume MWFRs were mostly small in all basins, despite the large magnitude of the changes in heat fluxes. The exceptions to this were the non-linear changes in the Atlantic MWFR fixed-volume heat content as a result of the largest magnitude perturbations (±100

Wm^{-2}), which were of similar magnitude to the linear changes, and the non-linear changes in the Indian MWFR fixed-volume heat, which started at a similar magnitude to the linear changes, although the linear changes grew larger after 8-9 years.

These results confirmed that the adjoint sensitivities can indeed successfully predict the linear impact of changes in surface forcings. In some regions, the sensitivities predicted the overall impact, even for relatively large perturbations, because the non-linear impacts were relatively small.

However, these results also highlighted a limitation of calculating adjoint sensitivities of the heat contents of fixed-volumes. As well as calculating the impact of the perturbations on the fixed-volume MWFRs (fix-MWFRs) of the adjoint experiments, we recalculated the volume of the MWFRs in the perturbation experiments, as the change in properties in the perturbation experiments impact not only the temperature of the MWFRs, but the depth of the mixed layer and SAMW source waters. These results showed, in some cases, that the varying-volume MWFRs (var-MWFRs) had opposite signed linear heat content changes to the fix-MWFRs. For example, in the Pacific sector, the var-MWFRs increased in heat content whilst the fix-MWFRs decreased in heat content. Further analysis revealed this was due to cooler fix-MWFRs resulting in a deepening of the mixed layer, and as such an increase in the volume of the recalculated var-MWFR, with an overall larger heat content. The opposite effect was found for warmer fix-MWFRs, which produced shallower mixed layers and so decreased the volume of the recalculated var-MWFR, with an overall lower heat content. The sometimes significant differences between the fix- and var-MWFRs highlights an important caveat when interpreting adjoint models. It must always be remembered that they show changes over a fixed volume, not a water mass or layer which may dynamically alter its thickness in response to forcing.

The second perturbation experiment was a step change of the zonal wind stress in the South-West Pacific, stretching east from New Zealand. This step change was in the form of a dipole, centered over the western section of northern boundary of the median location of the Pacific MWFR. The form of the dipole directly mirrored the ensemble mean sensitivity of the Pacific MWFR to zonal wind stress. This also relates to the results of Iudicone et al. (2007), who found that the Pacific basin-wide meridional pressure gradient is responsible for controlling the exchange of Antarctic Intermediate Water (AAIW) between the Southern and Pacific oceans in a numerical model. If the volume of AAIW changes, it can be expected that both the exchange and heat content will change, so the sensitivity of the Pacific MWFR heat content to this gradient via the wind stress may indicate the same process.

This perturbation experiment highlighted the influence of the bulk formulae on the surface properties in the model. Whilst linear, opposite-signed perturbations in zonal wind stress were applied in the two experiments, these resulted in significant *non-linear* anomalies in the surface heat flux, due to the actions of the bulk formulae. I.e. in both perturbation experiments, there was a similar, large decrease in the ocean to atmosphere heat flux across the perturbation region due to the increase in wind stress *magnitude*. This is an expected result of the local increase in SST when wind stress increases, but introduced a non-linear influence that meant the linear dependence of the MWFRs on wind stress could not be calculated directly via these perturbation experiments.

Nonetheless, the predicted linear responses in the Pacific and Indian fixed-volume heat contents were indeed found, with the non-linear impacts small in both volumes. The Atlantic MWFR was not predicted to have a high sensitivity to the wind stress changes, and accordingly the increase in heat content found was of an order of magnitude or two smaller than in the other basins, with similar magnitude linear and non-linear changes. Thus the influence of the non-linear anomalies in the surface heat flux are found to be minimal when looking at the fixed-volume heat content changes.

Unlike in the heat flux perturbation experiment, the change of heat content of the var-MWFRs was found to be of the same sign as the fix-MWFRs, i.e. both the fix-MWFR and the var-MWFR showed a linear increase in heat content for the positive-signed perturbation. However, the influence of the non-linear heat flux anomaly was apparent, as the non-linear changes were of similar magnitude to the linear changes, except during winter when the linear changes dominated. This was due to the non-linear heat flux anomaly producing the same increase in varying-volume heat content for both perturbations, which was seasonally of a similar order of magnitude to the linear impact of the wind stress perturbations.

The final perturbation experiment was designed to test a region notable for its lack of significant sensitivity – a region in the Indian ocean east of Africa and north of Madagascar. The meridional wind stress was perturbed here by fixed steps of two orders of magnitude larger than the climatological means for the region. This resulted in heat content changes in the MWFRs one to two orders of magnitude lower than in the previous perturbation experiments. The linear and non-linear impacts were of similar magnitude for both the fix-MWFR and var-MWFR, although as in the zonal wind stress perturbation there were non-linear anomalies in heat fluxes due to the action of the bulk formulae. This confirmed that the adjoint sensitivities were indeed accurate at locating regions of large linear sensitivity, and also implied that the non-linear sensitivity is relatively low in low linear sensitivity regions.

5.3 Discussion and Future Work

We have summarized here the behaviour of the adjoint sensitivities of the MWFRs in ECCOv4 r2. The only modification we have carried out is to scale the sensitivities by representative scalar standard deviations in order to compare sensitivities to different properties with one another. However, this is not the only choice that could have been made. Indeed, it is also informative to combine the adjoint sensitivities with other spatially varying fields. For example, convolving adjoint sensitivities to surface properties with two-dimensional, spatially varying, standard deviation fields can also be informative as it highlights not only where sensitivities are largest, but where variability is amplified by increased sensitivity. Conversely, a region with high sensitivity may be a region of low variability, and as such be less interesting to investigate. This might highlight where observational campaigns should be focused in order to accurately characterize the variability in a given surface forcing, where an adjoint may suggest there is a high sensitivity to such variability. Similarly, predicted changes in surface forcing under climate change scenarios may be expected to have greater impact if they occur over areas of high sensitivity.

Instead of looking at observed variability in a property, one might instead look at the spread in values between different numerical models, such as the CMIP climate model ensembles. Combining these with our adjoint sensitivities would inform on where model disagreement in surface forcings was expected to impact on predictions of MWFR heat content. This could provide motivation for model improvement in certain regions, or show which processes should be prioritized for development.

Additionally, one can combine sensitivity fields with anomaly (from climatological mean) fields in order to attribute changes in an objective function. In other words, if a particular year had an unusually large MWFR heat content compared with the climatological mean, one could attribute the linear contributions to this difference using the time varying adjoint sensitivities of surface properties convolved with the time varying anomalies of these properties.

The results as presented here have indicated the usefulness of adjoint models in predicting the linear sensitivity of regions of interest to surface fluxes and to interior properties. Of interest to the Southern Ocean research community are the findings that mode water formation regions appear to be as sensitive to non-local, dynamically linked, wind stress changes on multi-year timescales as to local, kinematically linked, heat flux changes on short time scales. Of interest to the ocean modeling community is the finding that the adjoint sensitivities can accurately predict the linear behaviour of perturbations to the heat content of fixed-volumes in the forward, non-linear model. However, there are timescales and regions where non-linear effects are as important, and care must be taken when interpreting results if the assumption of a fixed-volume is not representative of the expected behaviour.

A Appendix

A.1 Mask Comparison

Figure A.1 shows the domain integrated absolute sensitivities to surface properties for 1999, comparing the total sensitivity of the 1999 MWFRs as described in section 2 (red lines) with the sensitivity of the 1999 Jul-Nov maximum mixed layer depth for the whole of the Southern Ocean (south of 30°S). Thus the difference between the two objective functions is the horizontal extent – the MWFRs are restricted to the areas determined by low PV values and deep mixed layers, whereas the whole Southern Ocean mixed layer stretches across the domain in the horizontal.

The differences are most striking for the sensitivities to E-P-R, with the mixed layer sensitivities not showing the growth with increased lag that the MWFRs do, however both sensitivities remain extremely small relative to the others calculated. In general, for the heat flux and wind stress sensitivities, the mixed layer sensitivities peak at a similar or higher value at zero lag, and then decay faster with lag than the MWFR sensitivities. This is not surprising as the Southern Ocean mixed layer in general has a large surface area and is only on the order of ∼100m depth outside the MWFRs (see, for example, figure 1), and so it is expected that it will be most sensitive to recent forcings and quickly lose memory of the past. The absolute wind stress sensitivities in particular show far longer reaching behaviour for the MWFRs, likely due to the presence of dipoles along the boundaries of the MWFRs.

This demonstrates that the choice to restrict our objective functions to just the MWFRs themselves produces sensitivities with a richer range of behaviour and avoids over-focus on recent surface interactions.

A.2 Linear and Non-linear Component Derivation

Given a function $f(x)$ that is infinitely differentiable at a point a, the Taylor series is defined as:

$$f(x) = f(a) + (x-a)\frac{f'(a)}{1!} + (x-a)^2\frac{f''(a)}{2!} + (x-a)^3\frac{f'''(a)}{3!} + ..., \tag{A.1}$$

If we assume that the a given objective function value J is a function of the model surface forcings, defined by a state vector χ, i.e. $J \equiv J(\chi)$, and we consider perturbations to this state vector as $\Delta\chi$, then we can approximate the perturbed objective function as an expansion about the point χ using (A.1), i.e.

$$J(\chi + \Delta\chi) \approx J(\chi) + \Delta\chi J'(\chi) + (\Delta\chi)^2\frac{J''(\chi)}{2} + ..., \tag{A.2}$$

where we can identify $J'(\chi)$ with the linear component (which is estimated by the adjoint sensitivities $\partial J/\partial\chi$) and $J''(\chi)$ with the non-linear component of $J(\chi)$. Using (A.1) to similarly define $J(\chi - \Delta\chi)$, we can combine this with (A.2) to find:

$$\frac{J(\chi+\Delta\chi)}{2} - \frac{J(\chi-\Delta\chi)}{2} \approx \Delta\chi J'(\chi), \tag{A.3}$$

$$\frac{J(\chi+\Delta\chi)}{2} + \frac{J(\chi-\Delta\chi)}{2} - J(\chi) \approx (\Delta\chi)^2 \frac{J''(\chi)}{2}, \tag{A.4}$$

assuming that $J'''(\chi)$ and higher order terms $<<\ J(\chi), J'(\chi)$. Thus, by carrying out the perturbation experiments with state vectors $\chi \pm \Delta\chi$, we can estimate the linear and non-linear behaviour of the objective function and test this assumption. We can similarly identify any model variable as a function of the model surface forcings, and use the same method to combine results from the control and perturbation experiments to approximate the linear and non-linear behaviour of those model variables.

Acknowledgments

This study is supported by grants from the Natural Environment Research Council (NERC), including [1] The North Atlantic Climate System Integrated Study (ACSIS) (grant NE/N018028/1, author DJ), [2] Securing Multidisciplinary UndeRstanding and Prediction of Hiatus and Surge events (SMURPHS) (grant NE/N006038/1, author EB), and [3] Ocean Regulation of Climate by Heat and Carbon Sequestration and Transports (ORCHESTRA, grant NE/N018095/1, authors EB, AM). The ECCOv4-r2 model setup used in this work is available for download on Github (`https://github.com/gaelforget/ECCOv4`) as an instance of the MIT general circulation model (MITgcm, `http://mitgcm.org/`). Numerical model runs were carried out on ARCHER, the UK national HPC facility (`http://archer.ac.uk/`). Adjoint code was generated using the TAF software tool, created and maintained by FastOpt GmbH (`http://www.fastopt.com/`).

References

Adcroft, A., Campin, J.-M., Hill, C., & Marshall, J. (2004, dec). Implementation of an AtmosphereOcean General Circulation Model on the Expanded Spherical Cube. *Monthly Weather Review*, *132*(12), 2845–2863. Retrieved from `http://journals.ametsoc.org/doi/abs/10.1175/MWR2823.1` doi: 10.1175/MWR2823.1

Bindoff, N. L., & Mcdougall, T. J. (1994). Diagnosing climate change and ocean ventilation using hydrographic data. *Journal of Physical Oceanography*, *24*(6), 1137–1152.

Cerovečki, I., Meijers, A. J., Mazloff, M. R., Gille, S. T., Tamsitt, V. M., & Holland, P. R. (2019). The effects of enhanced sea ice export from the Ross sea on recent cooling and freshening of the Southeast Pacific. *Journal of Climate*, *32*(7), 2013–2035.

Close, S. E., Naveira Garabato, A. C., McDonagh, E. L., King, B. A., Biuw, M., & Boehme, L. (2013). Control of Mode and Intermediate Water Mass Properties in Drake Passage by the Amundsen Sea Low. *Journal of Climate*, *26*(14), 5102-5123. Retrieved from `https://doi.org/10.1175/JCLI-D-12-00346.1` doi: 10.1175/JCLI-D-12-00346.1

Forget, G., Campin, J.-M., Heimbach, P., Hill, C. N., Ponte, R. M., & Wunsch, C. (2015, oct). ECCO version 4: an integrated framework for non-linear inverse modeling and global ocean state estimation. *Geoscientific Model Development*, *8*(10), 3071–3104. Retrieved from `http://www.geosci-model-dev.net/8/3071/2015/` doi: 10.5194/gmd-8-3071-2015

Frölicher, T. L., Sarmiento, J. L., Paynter, D. J., Dunne, J. P., Krasting, J. P., & Winton, M. (2015, jan). Dominance of the Southern Ocean in Anthropogenic Carbon and Heat Uptake in CMIP5 Models. *Journal of Climate*, *28*(2), 862–886. Retrieved from `http://journals.ametsoc.org/doi/10.1175/JCLI-D-14-00117.1` doi: 10.1175/JCLI-D-14-00117.1

Gao, L., Rintoul, S. R., & Yu, W. (2018, jan). Recent wind-driven change in Subantarctic Mode Water and its impact on ocean heat storage. *Nature Climate Change*, *8*(1), 58–63. Retrieved from `http://dx.doi.org/10.1038/s41558-017-0022-8http://www.nature.com/articles/s41558-017-0022-8` doi: 10.1038/s41558-017-0022-8

Hanawa, K., & Talley, L. D. (2001). Chapter 5.4 Mode waters. In G. Siedler, J. Church, & J. Gould (Eds.), *Ocean circulation and climate* (Vol. 77, pp. 373–386). Academic Press. Retrieved from `http://www.sciencedirect.com/science/article/pii/S0074614201801297` doi: https://doi.org/10.1016/S0074-6142(01)80129-7

Iudicone, D., Rodgers, K. B., Schopp, R., & Madec, G. (2007, jan). An Exchange Window for the Injection of Antarctic Intermediate Water into the South Pacific. *Journal of Physical Oceanography*, *37*(1), 31–49. Retrieved from `http://journals.ametsoc.org/doi/abs/10.1175/JPO2985.1` doi: 10.1175/JPO2985.1

Jones, D. C., Boland, E. J. D., Meijers, A. J. S., Forget, G., Josey, S. A., Sallee, J.-B., & Shuckburgh, E. F. (2019a). The sensitivity of Southeast Pacific heat distribution to local and remote changes in ocean properties. *Journal of Physical Oceanography*(*under review*).

Jones, D. C., Boland, E. J. D., Meijers, A. J. S., Forget, G., Josey, S. A., Sallee, J.-B., & Shuckburgh, E. F. (2019b). What controls the heat content of the recently ventilated East Pacific sector of the Southern Ocean? *Journal of Geophysical Research: Oceans*(124). doi: 10.1029/2019JC015460

Jones, D. C., Forget, G., Sinha, B., Josey, S. A., Boland, E. J. D., Meijers, A. J. S., & Shuckburgh, E. (2018, apr). Local and Remote Influences on the Heat Content of the Labrador Sea: An Adjoint Sensitivity Study. *Journal of Geophysical Research: Oceans*, *123*(4), 2646–2667. Retrieved from `http://doi.wiley.com/10.1002/2018JC013774` doi: 10.1002/2018JC013774

Khatiwala, S., Tanhua, T., Mikaloff Fletcher, S., Gerber, M., Doney, S. C., Graven, H. D., ... Sabine, C. L. (2013, apr). Global ocean storage of anthropogenic carbon. *Biogeosciences*, *10*(4), 2169–2191. Retrieved from `https://www.biogeosciences.net/10/2169/2013/` doi: 10.5194/bg-10-2169-2013

Landschützer, P., Gruber, N., Haumann, F. A., Rödenbeck, C., Bakker, D. C., Van Heuven, S., ... Wanninkhof, R. (2015, sep). The reinvigoration of the Southern Ocean carbon sink. *Science*, *349*(6253), 1221–1224. Retrieved from `http://www.ncbi.nlm.nih.gov/pubmed/26359401` doi: 10.1126/science.aab2620

Le Quéré, C., Andrew, R. M., Friedlingstein, P., Sitch, S., Pongratz, J., Manning, A. C., ... Zhu, D. (2018, mar). Global Carbon Budget 2017. *Earth System Science Data*, *10*(1), 405–448. Retrieved from `https://www.earth-syst-sci-data.net/10/405/2018/` doi: 10.5194/essd-10-405-2018

Levitus, S., Antonov, J. I., Boyer, T. P., Baranova, O. K., Garcia, H. E., Locarnini, R. A., ... Zweng, M. M. (2012, may). World ocean heat content and thermosteric sea level change (0-2000 m), 1955-2010. *Geophysical Research Letters*, *39*(10). Retrieved from `http://doi.wiley.com/10.1029/2012GL051106` doi: 10.1029/2012GL051106

Lumpkin, R., & Speer, K. (2007, oct). Global Ocean Meridional Overturning. *Journal of Physical Oceanography*, *37*(10), 2550–2562. Retrieved from `http://journals.ametsoc.org/doi/abs/10.1175/JPO3130.1` doi: 10.1175/JPO3130.1

Marotzke, J., Giering, R., Zhang, K. Q., Stammer, D., Hill, C., & Lee, T. (1999). Construction of the adjoint MIT ocean general circulation model and application to Atlantic heat transport sensitivity. *Journal of Geophysical Research*, *104547*(15), 529–29. doi: 10.1029/1999JC900236

Marshall, J., & Speer, K. (2012). Closure of the meridional overturning circulation through southern ocean upwelling. *Nature Geoscience*, *5*(3), 171.

McDougall, T. J., & Barker, P. M. (2011). Getting started with TEOS-10 and the Gibbs Seawater (GSW) oceanographic toolbox. *SCOR/IAPSO WG*, *127*, 1–28.

Meijers, A., Cerovečki, I., King, B., & Tamsitt, V. (submitted). A see-saw in Pacific Subantarctic Mode Water formation driven by atmospheric modes. *Journal of Geophysical Research*.

Mikaloff Fletcher, S. E., Gruber, N., Jacobson, A. R., Doney, S. C., Dutkiewicz, S., Gerber, M., … Sarmiento, J. L. (2006, jun). Inverse estimates of anthropogenic CO 2 uptake, transport, and storage by the ocean. *Global Biogeochemical Cycles*, *20*(2). Retrieved from http://doi.wiley.com/10.1029/2005GB002530 doi: 10.1029/2005GB002530

Naveira Garabato, A. C., Jullion, L., Stevens, D. P., Heywood, K. J., & King, B. A. (2009). Variability of Subantarctic Mode Water and Antarctic Intermediate Water in the Drake Passage during the late-twentieth and early-twenty-first centuries. *Journal of Climate*, *22*(13), 3661–3688. doi: 10.1175/2009JCLI2621.1

Newman, L., Talley, L., Mazloff, M., Galton-Fenzi, B., Ackley, S., Heimbach, P., … Sparrow, M. (2015). *Southern Ocean community comment on the Year of Polar Prediction Implementation Plan, SOOS Report Series* (Tech. Rep. No. 2). Retrieved from http://www.soos.aq/

Rintoul, S. R., & England, M. H. (2002, may). Ekman Transport Dominates Local AirSea Fluxes in Driving Variability of Subantarctic Mode Water. *Journal of Physical Oceanography*, *32*(5), 1308–1321. Retrieved from http://journals.ametsoc.org/doi/abs/10.1175/1520-0485{\%}282002{\%}29032{\%}3C1308{\%}3AETDLAS{\%}3E2.0.CO{\%}3B2 doi: 10.1175/1520-0485(2002)032⟨1308:ETDLAS⟩2.0.CO;2

Roemmich, D., Church, J., Gilson, J., Monselesan, D., Sutton, P., & Wijffels, S. (2015). Unabated planetary warming and its ocean structure since 2006. *Nature climate change*, *5*(3), 240.

Sloyan, B. M., Talley, L. D., Chereskin, T. K., Fine, R., Holte, J., Sloyan, B. M., … Holte, J. (2010, jul). Antarctic Intermediate Water and Subantarctic Mode Water Formation in the Southeast Pacific: The Role of Turbulent Mixing. *Journal of Physical Oceanography*, *40*(7), 1558–1574. Retrieved from http://journals.ametsoc.org/doi/abs/10.1175/2010JPO4114.1 doi: 10.1175/2010JPO4114.1

Verdy, A., Mazloff, M. R., Cornuelle, B. D., Kim, S. Y., Verdy, A., Mazloff, M. R., … Kim, S. Y. (2014, jan). Wind-Driven Sea Level Variability on the California Coast: An Adjoint Sensitivity Analysis. *Journal of Physical Oceanography*, *44*(1), 297–318. Retrieved from http://journals.ametsoc.org/doi/abs/10.1175/JPO-D-13-018.1 doi: 10.1175/JPO-D-13-018.1

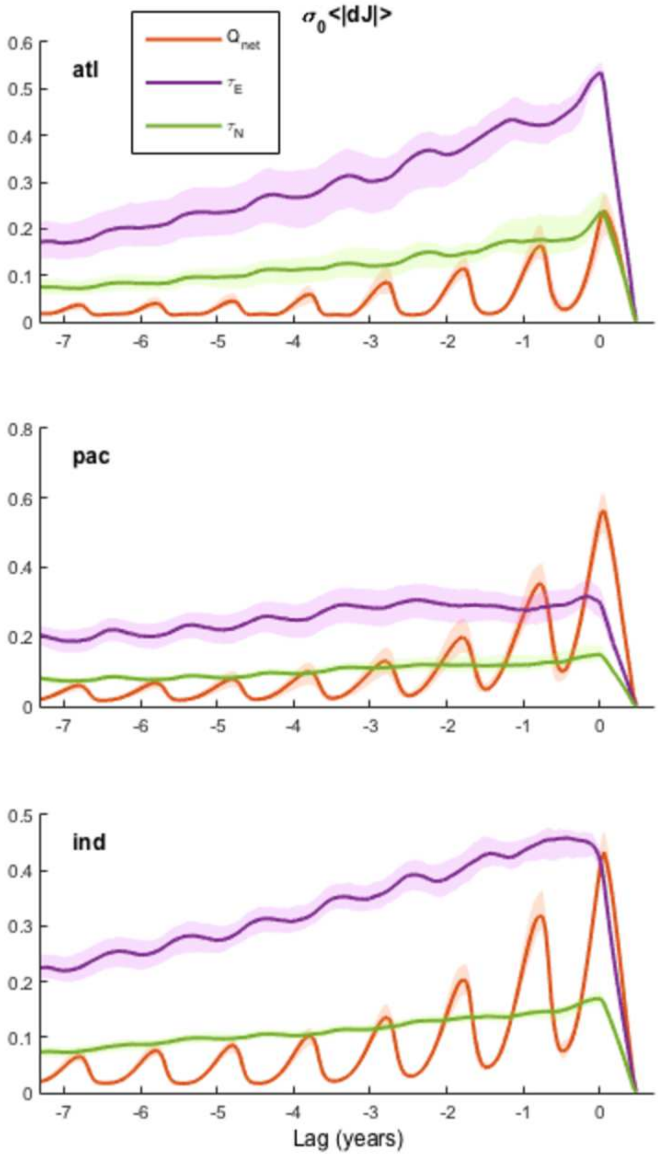

Figure 4. Wind stress largely dominates basin-integrated absolute sensitivities: Integrated absolute sensitivities to surface forcings by basin (top to bottom, as labeled), scaled by a representative standard deviation σ_0 and normalized, plotted against lag relative to the start of the objective function. Colors indicate surface net heat flux ($Q_{\rm net}$, red), and zonal/meridional wind stress ($\tau_{E/N}$, purple/green). The shaded area indicates the ensemble envelope (spanning the ensemble max and min values, *not* a standard deviation or similar) and thick lines the ensemble mean.

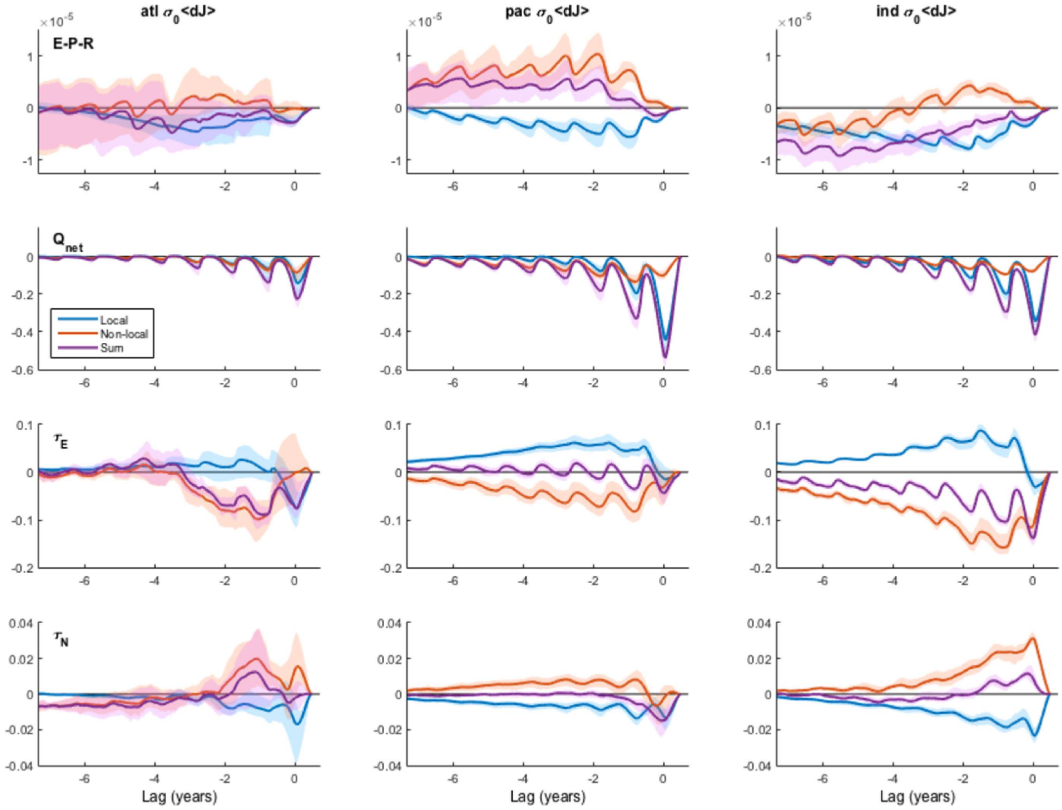

Figure 5. Local heat flux sensitivities dominate on short time scales, both local and non-local wind stress sensitivities are important at a range of time scales: Domain integrated sensitivities split by surface forcings (top to bottom, as labeled) and by basin (left to right, as labeled), scaled by a representative standard deviation and normalized, plotted against lag since the start of the objective function. Colors indicate the local sensitivities (within objective function mask, blue lines), non-local sensitivities (out-with mask, red lines) and the sum of the two, i.e./ total sensitivities (purple lines). The shaded area indicates the ensemble envelope (spanning the ensemble max and min values) and thick lines the ensemble mean.

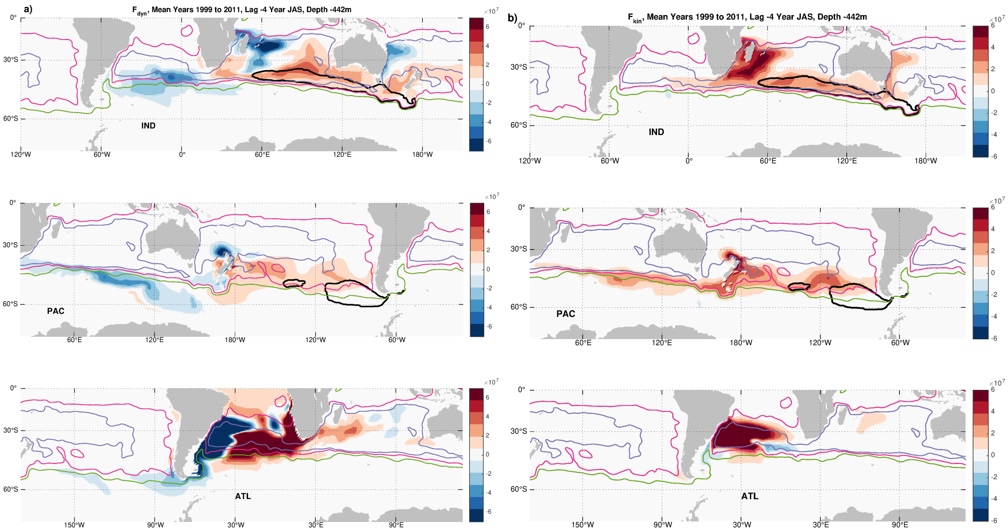

Figure 6. Example dynamic and kinematic sensitivities highlight their different properties: Sensitivities to a) dynamic and b) kinematic potential temperature changes at a fixed depth of -442m, fixed lag of 4 years, in all three basins (top to bottom). The black contour indicates the median location of the objective function at each depth, and as previously, the grey contours indicate the -17, 0, and 30 Sv mean barotropic streamlines. The associated ensemble standard deviations can be found in the supplementary information. Sensitivities are scaled by $1/\rho_0 c_p$ and are unitless.

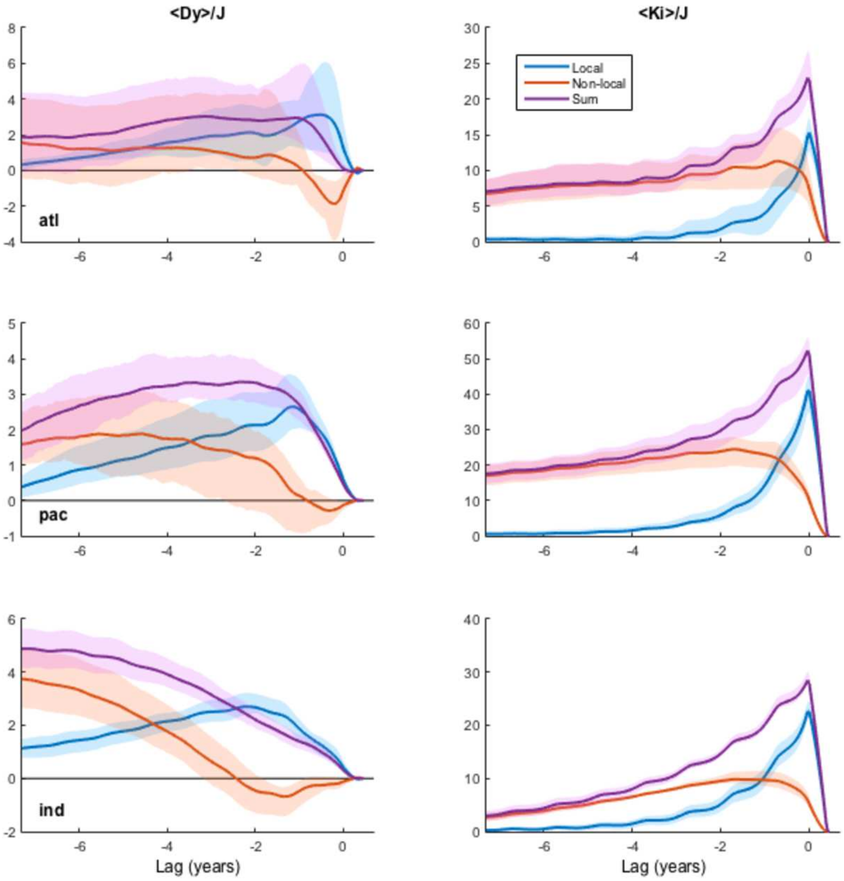

Figure 7. Domain-mean kinematic sensitivities decay over time, but dominate over domain-mean dynamic sensitivities, which show a basin-dependent structure: Domain-mean dynamic θ sensitivities (left), and domain-mean kinematic θ sensitivities (right) split by basin (top to bottom, as labeled). Colors indicate the contributions from local sensitivities (within objective function mask, blue lines), non-local sensitivities (out-with mask, red lines), and sum total sensitivities (purple lines). The shaded region indicates the envelope of individual ensembles, and thick lines the ensemble mean. All sensitivities have been scaled by J_b^Y and are therefore dimensionless.

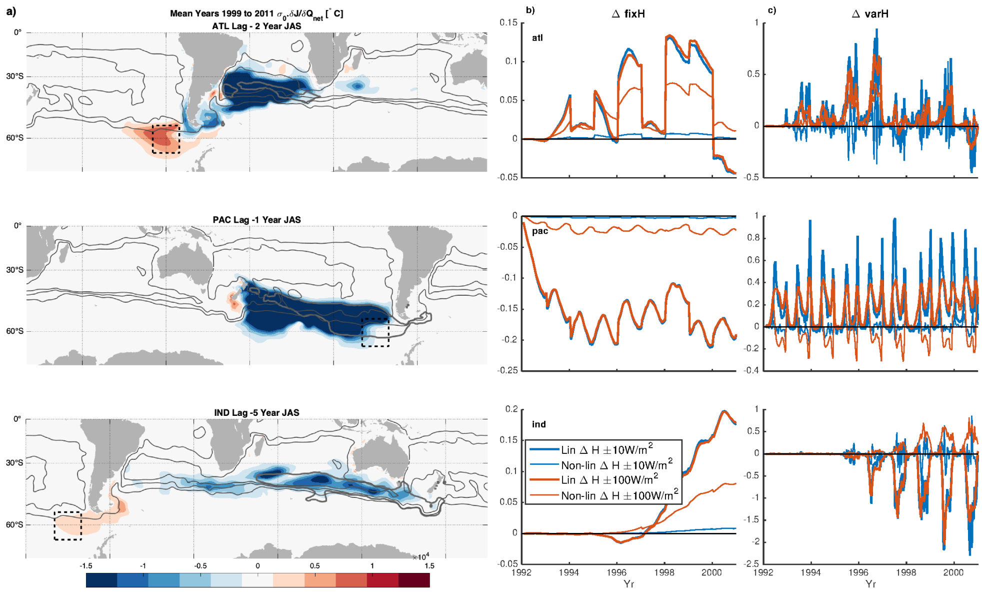

Figure 8. The adjoint sensitivities accurately predict the linear response of the fix-MWFRs heat content: a) Ensemble mean sensitivities of mode water heat content to $Q_{\rm net}$ in various basins at lags as labelled. Black contours indicated median location of objective functions, black dashed contour indicates location of $Q_{\rm net}$ perturbation (see text for details), grey contours, as before, indicate -17, 0, and 30 Sv mean SSH contours. Results of Pacific $Q_{\rm net}$ perturbation experiment, normalized linear (thick lines) and non-linear (thin lines) heat content changes divided by the perturbation magnitude, for either the fix-MWFR (b) or the var-MWFR (c), and for the $\pm$10W m^{-2} (blue) or $\pm$100W m^{-2} (red) experiments.

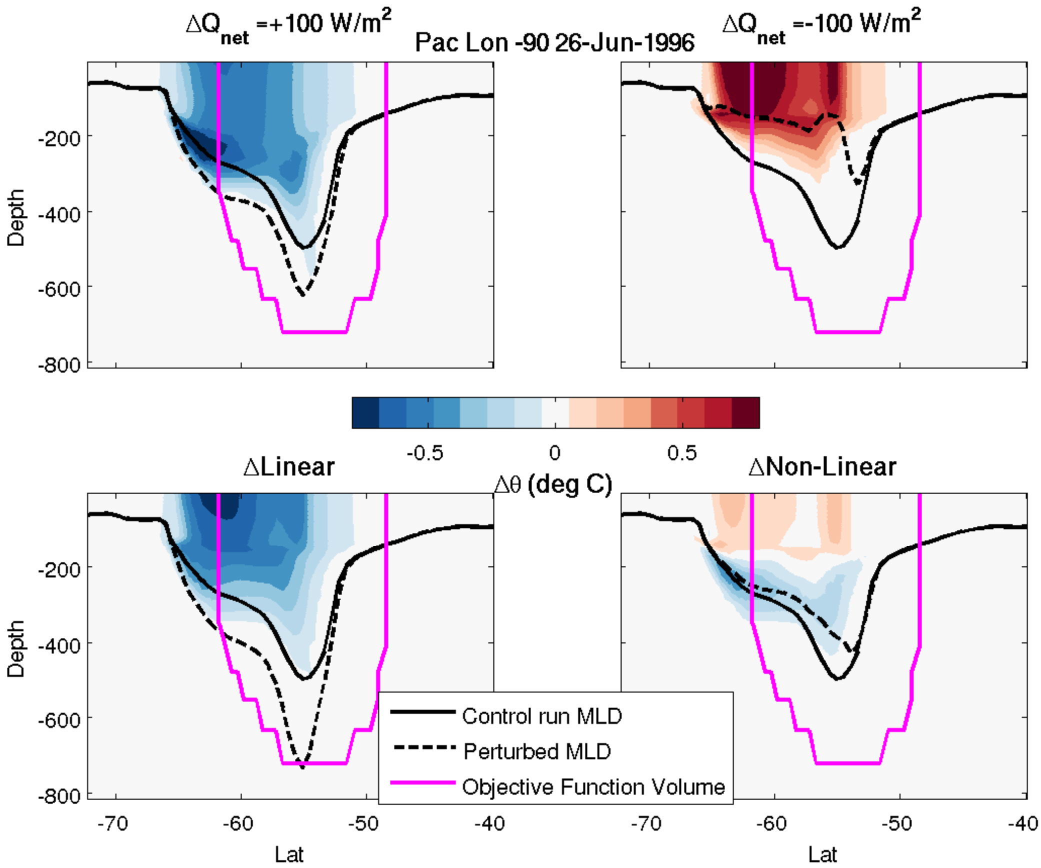

Figure 9. Linear changes in mixed layer depth act counter to linear changes in temperature, leading to opposite changes in heat content of the fix- and var-MWFRs: Latitude-depth snapshots of potential temperature changes (color) in the Pacific basin from the Pacific Q_{net} perturbation experiment in June 1996. Q_{net} is, as before, defined as positive from ocean to atmosphere. As labelled, the different panels show the difference from the control run for both positive and negative perturbations, and the combination of these to produce the linear and non-linear changes. The black solid lines show the control run instantaneous MLD and the magenta lines show the 1996 objective function volume (the same in every panel). The black dashed lines show the instantaneous MLD for the perturbation experiments as labelled.

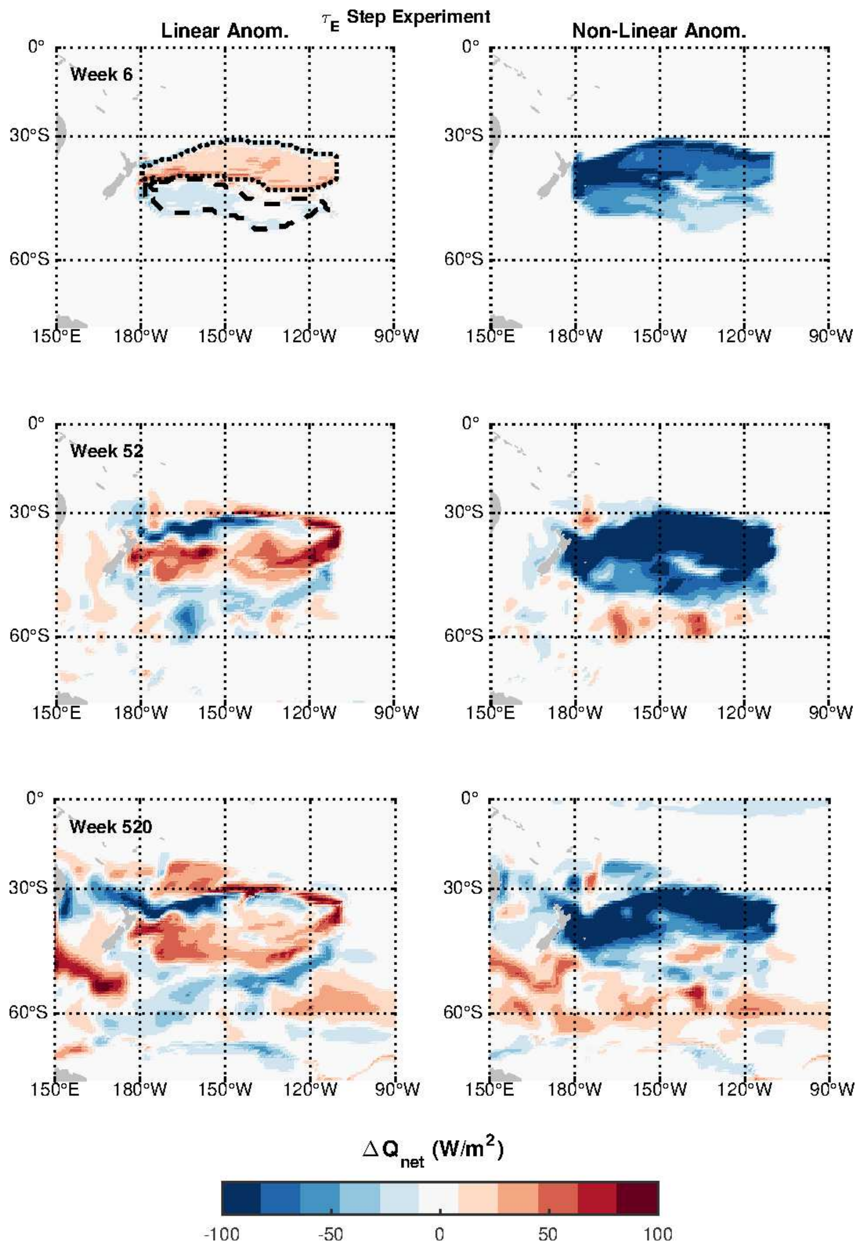

Figure 10. Comparison between applied wind stress and derived heat flux perturbations for Pacific experiment shows significant non-linear heat flux perturbations: Regions of applied Ocean τ_E perturbation ('positive' perturbation defined as $+1$ Nm^{-2} within dashed contour, -1 Nm^{-2} within dotted contour). Derived Ocean $Q_{\rm net}$ perturbations via bulk formulae, linear and non-linear components (color) going forward in time, top to bottom.

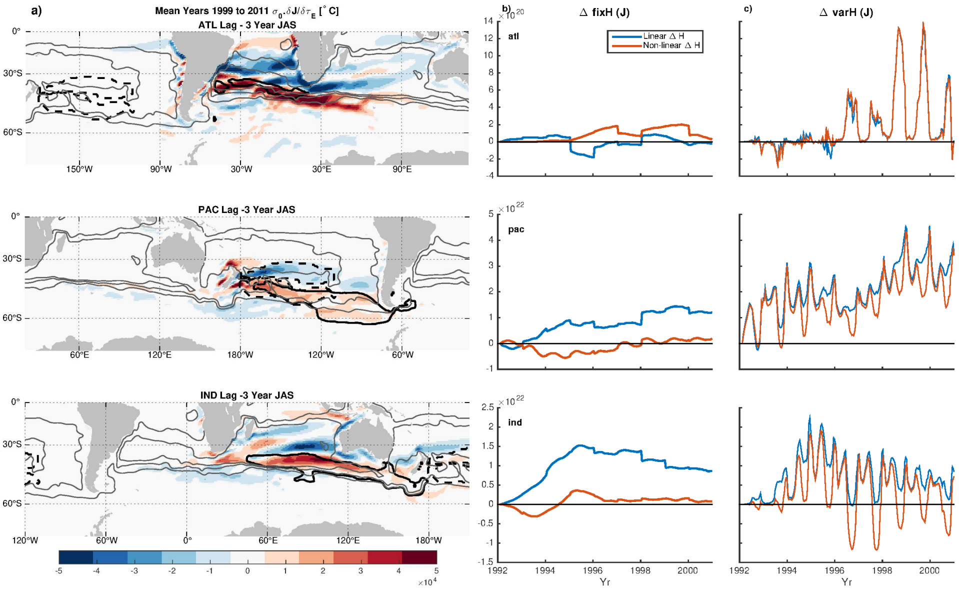

Figure 11. Left: Ensemble mean sensitivities of mode water heat content to τ_E in various basins in winter at 3 years lag as labelled. Black contours indicated median location of objective functions, black dashed contour indicates location of τ_E perturbation (see figure 10), grey contours, as before, indicate -17, 0, and 30 Sv mean SSH contours. Right: Results of Pacific τ_E perturbation experiment. Linear (blue lines) and non-linear (red lines) heat content changes, for either the fix-MWFR (b) or the var-MWFR (c). Positive signed linear/non-linear change indicates the changes resulting from the perturbation as depicted in figure 10.

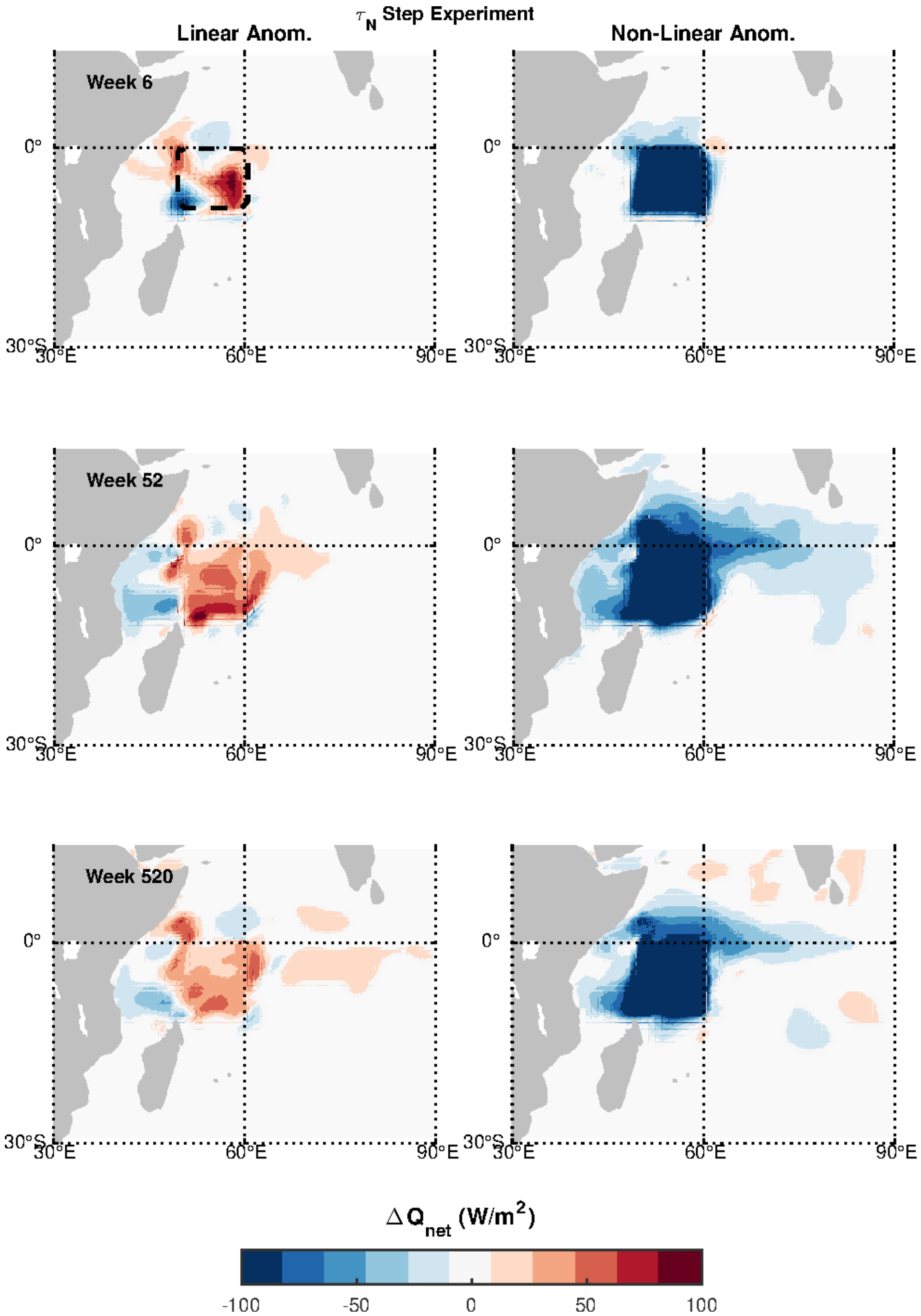

Figure 12. Comparison between applied wind stress and derived heat flux perturbations for E Africa experiment shows significant non-linear heat flux perturbations: Area of applied Ocean τ_N perturbation (± 1 Nm^{-2} within black dashed lines) and derived Ocean Q_{net} perturbations via bulk formulae, linear and non-linear components (color) going forward in time, top to bottom.

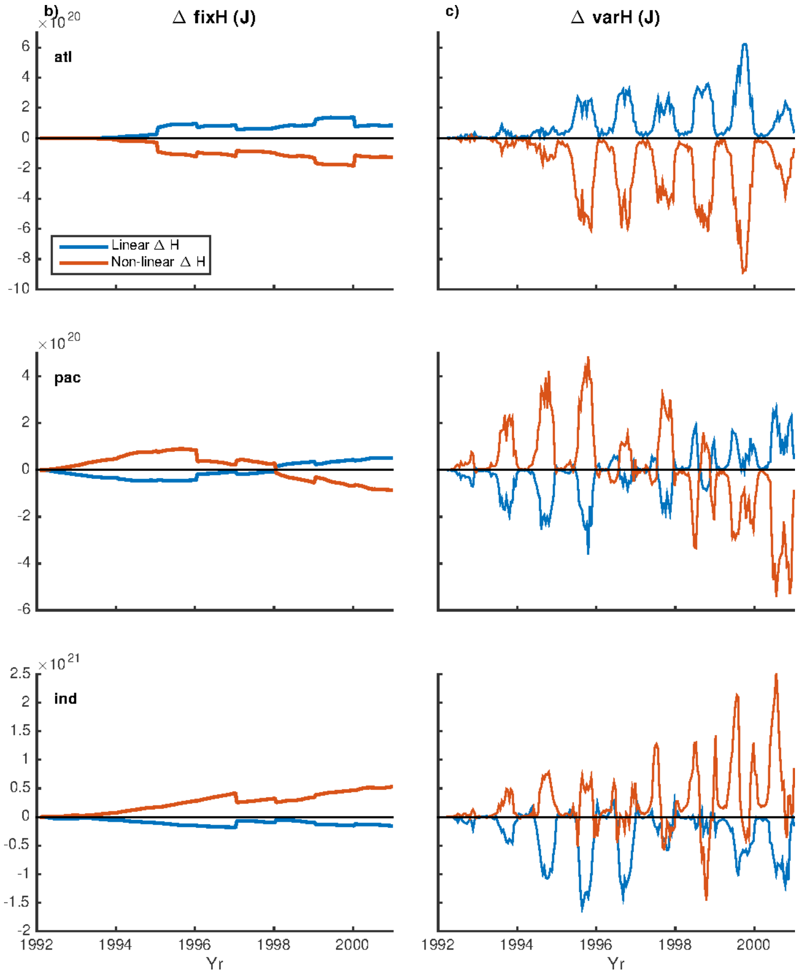

793 **Figure 13.** Results of E Africa τ_N perturbation experiment. Linear (blue lines) and non-
794 linear (red lines) heat content changes, for either the fix-MWFR (a) or the var-MWFR (b). Note
795 the different vertical scales when compared with figure 11

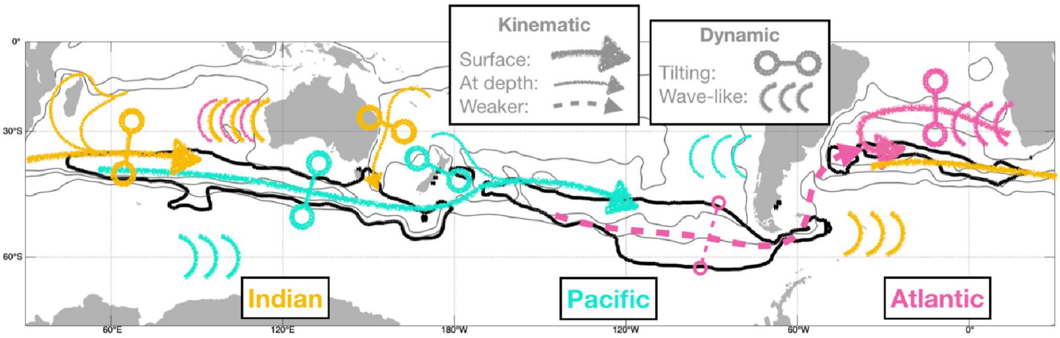

Figure 14. Schematic illustrating the main kinematic and dynamic sensitivities up to approximately 5 years lag for all three basins: Indian (yellow), Pacific (cyan), and Atlantic (pink). As before, thick black contours show the median location of the MWFRs and grey contours the -17, 0, and 30 Sv mean barotropic streamlines. Arrows indicate paths of kinematic sensitivities, with thinner lines indicating paths only found at depth and dotted lines showing relatively weaker paths. The circles connected by lines indicate where dynamic sensitivities resemble dipoles, where a change in isopycnal gradient will affect the MWFRs (the exact location of the symbols is not meaningful). Groups of curves indicate where wave-like patterns are found.

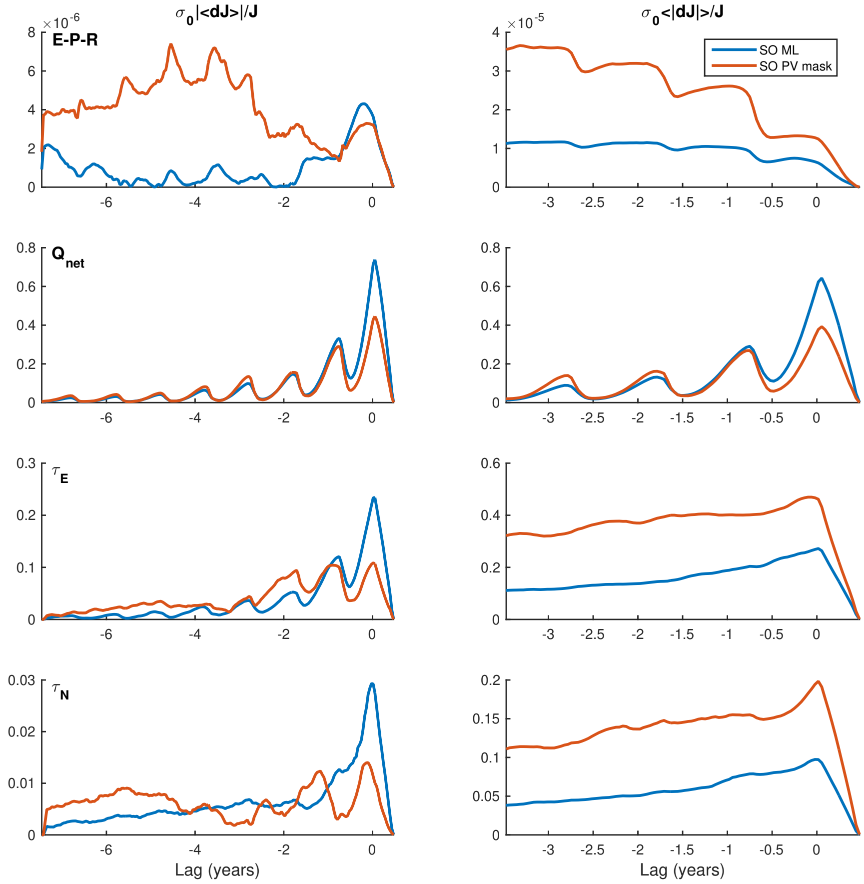

Figure A.1. Mean and absolute sensitivities (left and right hand plots respectively) to surface properties as labelled, salt water flux, heat flux, zonal, and meridional wind stress, top to bottom. Blue lines show an objective function of the whole Southern Ocean mixed layer depth Jul-Nov 1999 maximum. Red lines show an objective function of the whole Southern Ocean 1999 MWFRs – with the horizontal extent determined by the masks described in section 2 and the vertical extent the Jul-Nov maximum mixed layer depth. Sensitivities have been scaled by the representative standard deviations and the value of the objective function J, and then normalized.